# Ultra-Cold Bosons in One-Dimensional Single- and Double-Well Potentials

**Jake Steven Gulliksen**

A thesis submitted in partial fulfilment of
the requirements for the degree of
Masterate of Science at Massey University

Centre for Theorectical
Chemistry and Physics
Massey University
August 2010

# Ultra-Cold Bosons in One-Dimensional Single- and Double-Well Potentials

Jake Steven Gulliksen.

Thesis submitted for the degree of Masterate of Science
in Mathematical Physics at Massey University, September 2010.

## Abstract

A variationally optimised basis allows an accurate description of the quantum behaviour of ultra-cold atoms, even in the strongly correlated regime. A rescaling scheme corrects discrepancies caused by using a reduced Hilbert space. This approach also allows the modelling of experimentally realizable double-well potentials, which still reveals the maximally-entangled states seen in fixed basis models. Time dynamics of these double-well systems show macroscopic tunnelling between wells for bosons with a sufficient interaction strength.

The many-body problem of interacting bosons in the highly-correlated regime is difficult. The number of basis states needed to describe this quantum system accurately quickly grows beyond computational reach. Rescaling the interaction strength proves a simple and effective method of calculating exact eigenvalues in a reduced Hilbert space.

Bosonic systems in the double-well potential are investigated next. First, how different eigen-states depend on the interaction strength is examined. The variationally optimised method has advantages over a standard fixed basis method with the ability to model experimentally viable systems and explore more strongly-correlated regimes. Secondly, tunnelling dynamics in the double well are studied, specifically for a system where all particles initially occupy a single well. Oscillations corresponding to collective tunnelling between wells are found in regimes where there are zero interactions or bosons lie in a maximally-entangled state. What governs the dynamics outside these two regimes is also considered.

# Acknowledgements

First and foremost, I want to express my deep thanks to my supervisor, Prof. Joachim Brand. His insight, ideas, and attention to detail have been extremely valuable to me. With his guidance I have been able to get this thesis into its present form. I am also very thankful for the financial support he offered me, which made this project possible.

I am also indebted to Dr. David Hallwood, who has shown great patience despite my many questions. He has always been willing to sit down and assist with my research. Thanks also for the great discussions we have had and maybe one of these days I'll beat you at tennis!

I have really enjoyed studying here at Massey University. This is in no small part due to the people I work with, Thomas, Andy, Susan, and Renyuan. Thanks to Thomas, who first introduced me to the workings of the MCTDH software and answered any random physics questions I had. To Andy who has helped me with numerous computer problems and is always keen to debate an issue. To Susan and Renyuan who have both been great company.

Finally, I thank my wonderful wife Beccy. On many a night during my write up, she would bring dinner and keep me company. Also to my family and family-in-law, especially those who pretended to be interested in what I was doing.

People travel to wonder
at the height of the mountains,
at the huge waves of the seas,
at the long course of the rivers,
at the vast compass of the ocean,
at the circular motion of the stars,
and yet they pass by themselves
without wondering.
-*Augustine of Hippo*

# Contents

Chapter 1

# Introduction

In 1995, seventy years after its theoretical prediction, a Bose-Einstein condensate (BEC) was experimentally realised in a cloud of atoms [1, 2]. Here a gas of Rubidium atoms cooled to 170 nanoKelvin was found to macroscopically occupy the ground state. This sparked keen interest into the physics of ultra-cold atoms. Since then experimental methods have improved and BEC life-times in the order of tens of seconds have been reached [3]. BECs have been shown to be very useful in exhibiting quantum behaviour on a macroscopic scale. For instance, when confined to the double well they provide the means to observe quantum tunnelling [4]. Also, BECs have been recognised for their contribution to practical applications, for example in making precision measurements [5] and as a tool in quantum information [6].

This thesis is primarily concerned with one-dimensional (1D) systems. Restricting a BEC to one dimension can be realised experimentally [7] and holds interest for several reasons. Perhaps most intriguing is that we find phenomena not encountered in 2D or 3D, that is the gas of impenetrable bosons, or Tonks gas [8]. Furthermore it has been shown by Girardeau [9] that this provides us with an exactly soluble model for a 1D gas, useful for calibrating numerical results. Also, 1D systems make it possible to study larger numbers of atoms than is possible at higher dimensions due to computing restrictions.

In this thesis we present the multi-configurational time-dependent Hartree (MCTDH) approach to investigate the few-body spectrum and dynamics in the single- and double-well trapping potentials. This allows us to study highly-interacting regimes beyond the reach of mean field theory and extend work that has used a fixed basis method.

## 1.1 Indistinguishable Particles

In every day life we make use of the fact that particles (or objects) are distinguishable; for instance, you can distinguish your car from the Porsche over the fence. In the quantum mechanical world we find indistinguishable particles, which have the inherent property that they cannot be distinguished, even in principle. This makes the quantum mechanical world more attractive if you want to drive a car that looks like a Porsche. Unfortunately, examples of indistinguishable fundamental particles only fall into two categories, bosons and fermions.

We can understand why bosons and fermions have this property by seeing what makes particles distinguishable. The first way to distinguish classical particles is by their physical attributes, for example colour, size and charge. However, all electrons, for example, are electrons because they are particles which satisfy certain physical characteristics like a mass $m_e$ and charge $e$. Thus bosons and fermions are indistinguishable on this score. If we were to monitor the position and velocity of identical particles carefully we could track each trajectory and thus have the means to distinguish between them, even in a collision. This monitoring, however, is forbidden on a quantum scale by the Heisenberg uncertainty principle. That quantum particles are indistinguishable has a profound influence on their physics.

Consider two indistinguishable particles initially positioned at $\mathbf{r}_1$ and $\mathbf{r}_2$. In quantum mechanics the wave-function describing this system is

$$\Psi(\mathbf{r}_1, \mathbf{r}_2)\,, \tag{1.1}$$

which is associated with a set of physical observables. Because the particles are indistinguishable, we would expect that if the particles' positions were switched we would be left with the same set of observables. This is what we find, with the 'switching' operator $P_{ij}$ only adding a phase factor of $\pm 1$ because switching the same two particles twice must result in the original system. A many-body system may be described in one of two ways, the symmetric (+) or anti-symmetric (-) wavefunction.

$$P_{r_i r_j}\Psi(\dots, r_i, \dots, r_j, \dots) = \pm\Psi(\dots, r_i, \dots, r_j, \dots)\,. \tag{1.2}$$

Because bosons are particles with integer spin, then by the spin-statistics theorem we know they are described by the symmetric wave-function. Bosons will share quantum states which give rise to the phenomena of Bose-Einstein condensation

and superfluidity. Fermions as particles with half-integer spin are described with an anti-symmetric wave-function. It follows that the two-particle wave-function vanishes for two fermions in the same state. This condition is known as the Pauli exclusion principle and leads on to Fermi-Dirac statistics.

The statistics of particles with integer spin was first studied by Bose who derived statistics for photons. Bose sent this to Einstein who was impressed and extended Bose's idea to include matter. The resultant statistics is called Bose-Einstein statistics and was used to predict a phase change at very low temperatures known as Bose-Einstein condensation.

## 1.2 BEC Theory

The BEC transition is a statistical effect involving a system of bosons. In this section we summarise the main results discussed in detail in many statistical mechanics textbooks [10]. Consider $N$ non-interacting bosons of mass $m$ in thermal equilibrium at a temperature $T$. The mean population of a quantum state with energy $\varepsilon$ is given by the Bose-Einstein distribution function

$$n_i(\varepsilon_i, \mu, T) = \frac{1}{e^{(\varepsilon_i - \mu)/k_B T} - 1}\,, \tag{1.3}$$

where $k_B$ is Boltzmann's constant and $\mu$ is the chemical potential, or the energy required to add one more particle to the system. Given Eq. (1.3), we see that $\mu$ must be smaller than the lowest energy state $\varepsilon_0$ or we have a negative population which is a non-physical solution. In an homogeneous system the ground state is the state with zero momentum, thus $\varepsilon_0 = 0$ and $\mu_0$ must be negative for physical solutions. Furthermore as $\mu_0 \to 0^-$ we approach a singularity in Eq. (1.3). We will see this suggests that in this regime a large proportion of particles occupy the ground state.

The number of allowed energy states in an energy range $\varepsilon$ to $\varepsilon + \mathrm{d}\varepsilon$ is given by $g(\varepsilon)\,\mathrm{d}\varepsilon$. Here

$$g(\varepsilon) = C\varepsilon^{\alpha - 1} \tag{1.4}$$

is the density of states. The constants $C$ and $\alpha$ depend on the system parameters. For a system of free particles in $d$ dimensions, $\alpha = d/2$. If instead, the particles are confined to a d-dimensional harmonic trap, $\alpha = d$. We consider a three dimensional system confined to a volume $\Omega$, in which case $g(\varepsilon) = \frac{\Omega}{4\pi^2}\left(\frac{2m}{\hbar^2}\right)^{3/2}\varepsilon^{1/2}$.

In a system with a large number of atoms the total density $\rho$ can be written

$\rho = \rho_0 + \rho_e$, the addition of the ground state density ($\rho_0$) with the density of all other excited states,

$$\rho_e = \int g(\varepsilon) n_i(\varepsilon_i, \mu, T)\, \mathrm{d}\varepsilon\,. \tag{1.5}$$

Evaluating the integral in Eq. (1.5) the density of particles in the excited states is found to be

$$\rho_e = \zeta(3/2)(e^{\mu/k_B T})\Omega \left(\frac{m k_B T}{2\pi\hbar^2}\right)^{3/2}, \tag{1.6}$$

where $\zeta(3/2)$ is the Riemann zeta function. By Eq. (1.6) we see that the excited states are maximally populated at any given temperature when $\mu = 0$. We also see that there will be some temperature $T_c$ such that $\rho_0 \approx \rho$, that is, most particles will occupy the ground state. Rearranging Eq. (1.6) this critical temperature is found to be

$$T_c = \frac{2\pi\hbar^2}{k_B m}\left(\frac{\rho}{\zeta(3/2)}\right)^{2/3}. \tag{1.7}$$

In a gas well above $T_c$ few particles occupy the ground state, while the excited states are heavily populated. As the gas cools the number of available excited states decreases and continues to decrease through $T_c$. Below this temperature the gas forms a condensate by macroscopically occupying the ground state, known as a Bose-Einstein condensate.

Another, more intuitive way of understanding this concept is to consider the de Broglie wavelength of a single boson given by $\lambda = \sqrt{\frac{2\pi\hbar^2}{m k_B T}}$. We have a BEC when the wavelength of each particle becomes comparable to the inter-particle distance where quantum effects become important. This is formalised in the following condition for a BEC,

$$\lambda^3 \rho \geq \zeta(3/2) \approx 2.612\,, \tag{1.8}$$

## 1.3 BEC's in Other Dimensions

In this section we consider what effect reducing the dimensionality of the system has in the condensation of a non-interacting Bose gas in a harmonic trap. Condensation in a three-dimensional harmonic trap occurs when $T < T_{3D}$. The critical temperature,

$$k_B T_{3D} = \hbar\omega_{3D}\left[\frac{N}{\zeta(3)}\right]^{1/3} \approx 0.94\hbar\omega_{3D} N^{1/3}\,, \tag{1.9}$$

is found by evaluating Eq. (1.5) when $\mu = 0$, $T = T_{3D}$. Here $\omega_{3D} \equiv (\omega_x\omega_y\omega_z)^{1/3}$ and $\hbar\omega_x$, $\hbar\omega_y$, $\hbar\omega_z$ are the oscillator energies for each respective dimension.

In two dimensions, corresponding to $\alpha = 2$ in Eq. (1.4), condensation is achieved if the trapping frequency in the third dimension satisfies $\hbar\omega_{2D} \ll k_B T_{2D} < \hbar\omega_z$ where $\omega_{2D} \equiv (\omega_x \omega_y)^{1/2}$. The critical temperature for the 2D system is given by

$$k_B T_{2D} = \hbar\omega_{2D} \left[\frac{N}{\zeta(2)}\right]^{1/2} \approx 0.78 \hbar\omega_{2D} N^{1/2} \,. \tag{1.10}$$

In one dimension ($\alpha = 1$) the integral in Eq. (1.5) diverges, thus a BEC does not exist in the thermodynamic limit. However macroscopic occupation of the groundstate is possible provided $\omega$ in the longitudinal direction is much smaller than the trapping frequencies in the transverse directions, that is $\omega_x \ll \omega_\perp$. The temperature needed to achieve this state is approximately [11]

$$k_B T_{1D} \simeq \hbar\omega_x \frac{N}{\ln(N)} \,. \tag{1.11}$$

Thus when a Bose gas is confined to a harmonic potential with very large anisotropy we may loosely talk of a BEC in one or two dimensions.

Chapter 2

# Theory

So far we have presented some of the concepts that make ultra-cold atoms of so much interest. This thesis, in particular, is concerned with studying 1D systems of interacting bosons. Thus after a brief introduction into the Fock space formalism in Sec. 2.1, we outline how such a system may be created from a 3D ultra-cold gas (Sec. 2.2). In this chapter we also present some key aspects of the theory which underlies the results in this thesis. Sections 2.3 and 2.4 contain details of two exactly soluble models which we can use to calibrate our numerical calculations. All numerical calculations in this thesis are made using the MCTDH approach, so in Sec. 2.5 we outline the basic theory of MCTDH and discuss two other methods that provide a valuable theoretical background. Finally in Sections 2.6 and 2.7 we review two papers that contain work which will be discussed in chapters 4 and 5 respectively.

## 2.1 Fock Space

Because we are dealing with a system of indistinguishable particles, keeping track of individual particles is no longer important (or possible). Rather, we are interested in what states are occupied. For this reason we introduce the Fock space, summarised here but found in many quantum mechanics textbooks such as [12]. The Fock space is defined as the direct sum of tensor products which are all copies of a single particle Hilbert space $H$.

$$F(H) = \bigoplus_{n=0}^{\infty} S_+ H^{\otimes n} = C \oplus H \oplus (S_+(H \otimes H)) \oplus (S_+(H \otimes H \otimes H)) \oplus \dots , \quad (2.1)$$

where $C$ is the zero body Hilbert space and $S_+$ is the operator that symmetries the space. A particularly useful basis called the occupation number basis counts the number of particles ($n_k$) occupying the state $\phi_k$. This information is contained in the number state $|\mathbf{n}\rangle$, which reads

$$|\mathbf{n}\rangle = |n_1, n_2, \ldots, n_k, \ldots\rangle. \tag{2.2}$$

The creation ($a^\dagger$) and annihilation ($a$) operators,

$$\begin{aligned} a_i^\dagger|\ldots, n_i, \ldots\rangle &= \sqrt{n_i+1}\,|\ldots, n_i+1, \ldots\rangle \\ a_i|\ldots, n_i, \ldots\rangle &= \begin{cases} \sqrt{n_i}\,|\ldots, n_i-1, \ldots\rangle & \text{for } n_i \geq 1, \\ 0 & \text{for } n_i = 0 \end{cases}, \end{aligned} \tag{2.3}$$

add or remove one particle in the $i^{th}$ state respectively. They obey the following commutation relations:

$$\begin{aligned} [a_i, a_j] &= [a_i^\dagger, a_j^\dagger] = 0 \\ [a_i, a_j^\dagger] &= \delta_{ij}\,. \end{aligned} \tag{2.4}$$

We also define the number operator $\hat{n}_i := a_i^\dagger a_i$, such that $\hat{n}_i|\mathbf{n}\rangle = n_i|\mathbf{n}\rangle$. This allows us to rewrite Eq. (2.2) and create any member of the occupation number basis via

$$|\mathbf{n}\rangle = \left(\prod_k \frac{1}{\sqrt{n_k!}}(a_k^\dagger)^{n_k}\right)|vac\rangle\,, \tag{2.5}$$

where $a_i|vac\rangle = 0$.

## 2.2 Modelling a One-Dimensional System

We consider $N$ interacting bosons of mass $m$ confined to a tight waveguide. A typical waveguide potential is the cigar shaped trap studied by Olshanii [13] which has an axially-symmetric 2D harmonic potential of frequency $\omega_\perp$. Dynamics in these transverse directions are essentially frozen out by cooling the system below $\hbar\omega_\perp$ thus leaving atomic motion purely along the longitudinal axis. The many-body Hamiltonian describing this system may be written

$$H = \sum_{i=1}^{N} h(p_i, x_i) + \sum_{i<j} V(x_i, x_j)\,, \tag{2.6}$$

where $h(p,x)$ is the single-particle Hamiltonian which includes kinetic energy and an external trapping potential and $V(x_i,x_j)$ is the effective interaction between particles. Because we assume that the system is dilute only two-body collisions are considered. We may approximate ultra-cold atoms to interact via a one-dimensional delta potential [13] and so the interaction potential becomes

$$V(x_i,x_j) = g_{1D}\delta(x_i - x_j)\,, \tag{2.7}$$

where the coupling strength is written entirely in terms of the system parameters

$$g_{1D} = \frac{2\hbar^2 a}{m a_\perp}\left(a_\perp - \mathcal{C}a\right)^{-1}\,,\ \mathcal{C} = 1.0326\ldots \tag{2.8}$$

Here $a_\perp = \sqrt{\hbar/m\omega_\perp}$ is the transverse harmonic oscillator length and $a$ is the s-wave scattering length. For negative values of $a$ the interaction is attractive while positive values of $a$ indicate repulsive interactions and are the subject of this thesis. From here on in we will only be considering a 1D system so $g_{1D}$ can lose the subscript.

Two boundary cases immediately present themselves, $g = 0$ and $g \to \infty$. The former is the trivial ideal gas while in the limit of the latter we find the realisation of a model unique to 1D systems, fermionization of bosons.

## 2.3 Tonks-Girardeau

In 1960 Girardeau showed that there is a one-to-one correspondence between the system of one-dimensional impenetrable bosons and spinless fermions [9]. This system of bosons, the so-called Tonks-Girardeau gas, amounts to taking $g \to \infty$ in the interaction term of Eq. (2.6). More formally it imposes the following hardcore boundary condition on the bosonic wave-function,

$$\Psi_B(\ldots x_i \ldots x_j \ldots) = 0 \qquad \text{if } |x_i - x_j| = 0\,, \tag{2.9}$$

which is equivalent to the Pauli exclusion principle which governs fermions. Girardeau proved that this many-body wave-function may be described as

$$\Psi_B = \mathcal{A}\Psi_F\,, \tag{2.10}$$

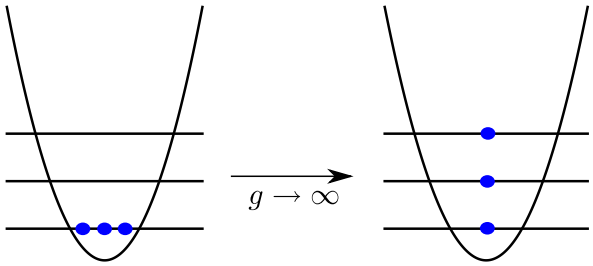


Figure 2.1: Sketch depicting the fermionization of bosons.

where

$$\mathcal{A} = \prod_{j>i} \mathrm{sgn}(x_j - x_i) \tag{2.11}$$

is the unit antisymmetric function [9] which only takes the values $\pm 1$ and $\Psi_F$ is the wave-function of $N$ non-interacting fermions governed by the single-particle Hamiltonian $h(p, x)$ of the previous section.

We can make a few deductions from the result above. In the ground-state Eq. (2.10) reduces to $\Psi_B = |\Psi_F|$, from which we can conclude that in the Tonks-Girardeau regime bosons become fermionized (Fig 2.1). Also because $|\mathcal{A}| = 1$ it follows that $\rho_B(x) = \rho_F(x)$ where $\rho(x)$ is the single particle density, that is the probability of finding a particle at $x$.

## 2.4 Two Bosons in a Harmonic Trap

Few soluble models exist that describe correlated systems with more than two particles. However, the simple model of two particles in a harmonic trap already exhibits the interplay between two-body interactions and the external potential. Two bosons of mass $m$ confined to a one-dimensional harmonic potential of frequency $\omega$ is described by the Hamiltonian

$$H = -\frac{\hbar^2}{2m}\left(\frac{\partial^2}{\partial x_1^2} + \frac{\partial^2}{\partial x_2^2}\right) + \frac{m\omega^2}{2}\left(x_1^2 + x_2^2\right) + g\delta(x_2 - x_1)\,, \tag{2.12}$$

where a point-like interaction is assumed, modelled by the Dirac delta function. We move from a position to a relative coordinate system with $R = \sqrt{1/2}(x_1 + x_2)$, the

centre of mass (com) coordinate and $r = \sqrt{1/2}(x_2 - x_1)$, the relative coordinate[1]. With a few lines of algebra we find $H = H_R + H_r$, where

$$H_R = -\frac{\hbar^2}{2m}\frac{d^2}{dR^2} + \frac{m\omega^2}{2}R^2 \;=\; H_{osc}(R) \tag{2.13a}$$

$$H_r = -\frac{\hbar^2}{2m}\frac{d^2}{dr^2} + \frac{m\omega^2}{2}r^2 + g\delta(r) \;=\; H_{osc}(r) + g\delta(r)\,. \tag{2.13b}$$

Eq. (2.13a) is simply the well understood Hamiltonian for a harmonic oscillator (denoted $H_{osc}$). It is left to solve the following Schrodinger equation,

$$\left(H_{osc}(r) + g\delta(r)\right)\Psi(r) = E\Psi(r)\,. \tag{2.14}$$

The eigen-states of Eq. (2.14) are discussed at length in [14] and further details may be found in [15]. For consistency with these papers we rescale all lengths in units of $r_0 = \sqrt{\hbar/m\omega}$ and energies in terms of $E_0 = \hbar\omega$. This leads to a new scaled length $\tilde{r} = r/r_0$, rescaled interaction strength $\tilde{g} = (\hbar\omega r_0)^{-1}g$, and rescaled energy $\tilde{E_n} = E_n/E_0$. The odd eigen-functions of Eq. (2.14) are

$$\tilde{\Psi}_n(\tilde{r}) = \mathcal{N}_n\mathcal{H}_n(\tilde{r})e^{-\frac{\tilde{r}^2}{2}}, \quad n = 1, 3, 5, \ldots\,, \tag{2.15}$$

where $\mathcal{H}_n(\tilde{r})$ are the Hermite polynomials and $\mathcal{N}_n$ is the associated normalisation constant. This of course is just the odd eigen-functions of the harmonic oscillator with well known eigen-values. On the other hand the even eigen-functions depend on $\tilde{g}$ and are found to be

$$\tilde{\Psi}_n(\tilde{r}) = \mathcal{N}_n e^{-\frac{\tilde{r}^2}{2}} U\left(\frac{1}{4} - \frac{\tilde{E_n}}{2}, \frac{1}{2}, \tilde{r}^2\right), \quad n = 0, 2, 4, \ldots\,, \tag{2.16}$$

where $U(a, b, z)$ is the Kummer function [16]. The corresponding eigen-values are given implicitly by

$$\tilde{g} = 2\sqrt{2}\frac{\Gamma\left(-\frac{\tilde{E_n}}{2} + \frac{3}{4}\right)}{\Gamma\left(-\frac{\tilde{E_n}}{2} + \frac{1}{4}\right)}\,. \tag{2.17}$$

The energy of each even eigen-state increases with $\tilde{g}$ and, as an example of fermionization, converges to the next higher lying odd eigen-value as $\tilde{g} \to \infty$.

[1] Of course the true center-of-mass coordinate is given by $R/\sqrt{2} = 1/2(x_1 + x_2)$ and $\sqrt{2}r = (x_2 - x_1)$ yields the true postion of atom 2 relative to atom 1. However, the factors of $\sqrt{2}$ were added so that the effective masses for the centre-of-mass motion and the relative motion are the same [14].

## 2.5 Methods

This thesis seeks to solve the time-dependent Schrödinger equation for a few ultracold atoms,

$$i\hbar\frac{\partial\Psi}{\partial t} = H(t)\Psi\,, \tag{2.18}$$

which is a non-trivial problem. Results in this thesis have been obtained using the multi-configurational time-dependent Hartree (MCTDH) ansatz for the wavefunction which will be discussed in section 2.5.3. This section will also discuss other many-body methods, both to understand previous work on this problem and to compare the MCTDH approach. A nice discussion of these methods may be found in [17].

### 2.5.1 Gross-Pitaevskii

By far the most basic many-body method assumes that all particles occupy the ground-state. In the zero temperature limit then we may assume that the $N$-particle wave-function is the product of $N$ ground-state single-particle orbitals, that is

$$\Psi_{GP}(x_1, x_2, \ldots, x_N) = \prod_{i=1}^{N}\phi(x_i)\,. \tag{2.19}$$

The Gross-Pitaevskii energy functional is found by taking the expectation value of the Hamiltonian (Eq. (2.6)),

$$\begin{aligned} E[\phi,\phi^*] &= \langle\Psi_{GP}|H|\Psi_{GP}\rangle \\ &= \int \mathrm{d}x\left[\frac{\hbar^2}{2m}|\nabla\phi|^2 + V_{ext}(x)|\phi|^2 + \frac{g(N-1)}{2}|\phi|^4\right]. \end{aligned} \tag{2.20}$$

With $E[\phi,\phi^*]$ it is now possible to find an upper bound for the groundstate energy [18]. This is done by looking for an extremum of $\partial(E-\mu\langle\psi_{GP}|\psi_{GP}\rangle) = 0$, where $\mu$ is the chemical potential, the energy required to add one particle to the system. This yields the time-independent Gross-Pitaevskii equation,

$$\mu\phi = \left(h + (N-1)g|\phi|^2\right)\phi\,. \tag{2.21}$$

We may also include time-dependence by introducing the action

$$A[\phi,\phi^*] = -\hbar\int \mathrm{d}x\,\mathrm{d}t\left[\phi^*\frac{\partial}{\partial t}\phi\right] + E[\phi,\phi^*]\,. \tag{2.22}$$

We find [19]

$$i\hbar\frac{\partial\phi}{\partial t} = \left(h + (N-1)g|\phi|^2\right)\phi\,. \tag{2.23}$$

### 2.5.2 Standard Method

The most straightforward approach to solving the time-dependent Schrödinger equation is by first expanding the $p$-dimensional wave-function into a direct product basis,

$$\Psi(Q_1,\ldots,Q_p,t) = \sum_{j_1=1}^{n_1}\cdots\sum_{j_p=1}^{n_p} C_{j_1\ldots j_p}(t)\prod_{\kappa=1}^{p}\varphi_{j_\kappa}^{\kappa}(Q_\kappa)\,, \tag{2.24}$$

where $n_\kappa$ is the number of stationary basis functions associated with the $\kappa^{th}$ degree of freedom (DOF), and the vector $C$ indexes each configuration. Then by applying the Dirac-Frenkel variational principle we find the following equations of motion,

$$i\dot{C}_{j_1,\ldots,j_p} = \sum_{l_1,\ldots,l_p}\langle\varphi_{j_1}^{(1)},\ldots,\varphi_{j_p}^{(p)}|H|\varphi_{j_1}^{(1)},\ldots,\varphi_{j_p}^{(p)}\rangle C_{l_1,\ldots,l_p}\,. \tag{2.25}$$

This method works well but struggles due to computing restrictions when the number of DOFs becomes larger than six.

### 2.5.3 MCTDH

The underlying idea behind the MCTDH approach is to introduce time dependence into the the single-particle functions of the standard model. The MCTDH method has been discussed at length in two review articles [20, 21]. Here we only give an overview, which is also found in [17]. We use the following ansatz to solve Eq. (2.18) for a physical system with $p$ degrees of freedom described by the coordinates $Q_1,\ldots,Q_p$,

$$\begin{aligned}\Psi(Q_1,\ldots,Q_p,t) &= \sum_{j_1=1}^{n_1}\cdots\sum_{j_p=1}^{n_p} A_{j_1\ldots j_p}(t)\prod_{\kappa=1}^{p}\varphi_{j_\kappa}^{\kappa}(Q_\kappa,t)\\ &= \sum_{J} A_J\Phi_J\,,\end{aligned} \tag{2.26}$$

where the vector $A$ indexes the configuration and $n_\kappa$ is the number of single-particle functions ($\varphi_{j_\kappa}^{\kappa}$) associated with the $\kappa^{th}$ DOF. Thus Eq. (2.26) is the Hartree product expansion of $p$ sets of orthonormal basis functions $\varphi^\kappa$. In Eq. (2.26) we use the collective index $J = j_1,\ldots,j_p$ and Hartree product $\Phi$ to tidy the notation.

The Dirac-Frenkel principle is applied to the ansatz above and we arrive at the following equations of motion [20],

$$i\dot{\mathbf{A}} = \mathcal{K}\mathbf{A} \tag{2.27a}$$

$$i\dot{\varphi}^{(\kappa)} = \left(1 - P^{(\kappa)}\right)\left(\rho^{(\kappa)}\right)^{-1}\mathcal{H}^{(\kappa)}\varphi^{(\kappa)}\,, \tag{2.27b}$$

where the coefficients $\mathbf{A}$ are now in matrix form, $\varphi^{(\kappa)} = (\varphi_1^{(\kappa)}, \cdots, \varphi_{n_\kappa}^{(\kappa)})^T$ is a vector, and the matrix

$$\mathcal{K}_{JL} = \langle \Phi_J | H | \Phi_L \rangle \tag{2.28}$$

is the Hamiltonian operator in terms of Hartree products. We have also introduced three new entities, $P$, $\rho$, and $\mathcal{H}$, which are described as follows. The projector $P$ projects into the space spanned by the single particle functions (SPFs) and so has the form

$$P^{(\kappa)} = \sum_j |\varphi_j^{(\kappa)}\rangle\langle\varphi_j^{(\kappa)}| \tag{2.29}$$

The operator $\left(1 - P^{(\kappa)}\right)$ ensures that the time derivative of the SPFs are orthogonal to the space spanned by the SPFs. This means that if the basis is spanned by the given SPFs then the SPFs become independent of time. If not then the variational principle will find the SPFs that best describes the wave-packet. For the other two entities we introduce the single hole function $\Psi_a^{(\kappa)}$.

The single-hole function ($\Psi_a^{(\kappa)}$) is found by integrating out the $\kappa^{th}$ degree of freedom from the Hartree product, that is

$$\Psi = \sum_a |\varphi_a^{(\kappa)}\rangle\langle\varphi_a^{(\kappa)}|\Psi\rangle = \sum_a \varphi_a^{(\kappa)}\Psi_a^{(\kappa)}\,, \tag{2.30}$$

and is described by the expression

$$\begin{aligned}\Psi_a^{(\kappa)} &= \sum_{j_1}\cdots\sum_{j_\kappa-1}\sum_{j_\kappa+1}\cdots\sum_{j_p} A_{j_1\cdots j_{\kappa-1}aj_{\kappa+1}\cdots j_p}\varphi_{j_1}^{(1)}\cdots\varphi_{j_{\kappa-1}}^{(\kappa-1)}\varphi_{j_{\kappa+1}}^{(\kappa+1)}\cdots\varphi_{j_p}^{(p)} \\ &= \sum_{J^\kappa} A_{J_a^{(\kappa)}}\Phi_{J^\kappa}\,,\end{aligned} \tag{2.31}$$

where the single-hole index $J_a^{(\kappa)}$ takes every value aside from $j_\kappa$, which it replaces with the constant $a$. The index $J^\kappa$ is similar to $J$ but removes the $\kappa^{th}$ entry. The mean field operator matrix $\mathcal{H}^{(\kappa)}$, analogous to the mean fields seen in Hartree-Fock theory, is written

$$\mathcal{H}_{ab}^{(\kappa)} = \langle\Psi_a^{(\kappa)}|H|\Psi_b^{(\kappa)}\rangle\,. \tag{2.32}$$

The density matrix $\rho^{(\kappa)}$ may also be written in terms of $\Psi_a^{(\kappa)}$,

$$\begin{aligned} \rho_{ab}^{(\kappa)} &= \langle \Psi_a^{(\kappa)} | \Psi_b^{(\kappa)} \rangle \\ &= \sum_{J^\kappa} A^*_{J_a^\kappa} A_{J_b^\kappa} \,. \end{aligned} \tag{2.33}$$

## 2.6 Ultra-Cold Bosons in a Double-Well Potential

In this section we will review a paper by Carr et. al. [22] which is very much related to the content of this thesis. This section begins by introducing the two-level Bose-Hubbard model, a standard fixed basis model. It closes by discussing two results which will be tested in chapter 4.

The general quantised Hamiltonian for $N$ bosons of mass $m$ interacting via the Dirac delta function in an external potential $V(x)$ is

$$H = \int \mathrm{d}x\, \hat{\Psi}^\dagger(x) \left( -\frac{\hbar^2}{2m}\frac{d^2}{dx^2} + V(x) \right) \hat{\Psi}(x) \;+\; \frac{g}{2} \int \mathrm{d}x\, \hat{\Psi}^\dagger(x) \hat{\Psi}^\dagger(x) \hat{\Psi}(x) \hat{\Psi}(x) \,, \tag{2.34}$$

where $\hat{\Psi}^\dagger(x)$ and $\hat{\Psi}(x)$ are the creation and annihilation field operators respectively. In [22], Carr et. al. consider such a system, where

$$V(x) = V_0 \left( \frac{16}{a^4} x^4 - \frac{8}{a^2} x^2 + 1 \right) \tag{2.35}$$

is a Duffing double-well potential which has two minima at $x = \pm a/2$ equal to zero and a maximum at $x = 0$ equal to $V_0$. We now expand the field operators into the basis of on-well localised wave-functions $\psi^l(x - x_j)$, composed from appropriate superpositions of eigen-functions of the single-particle Hamiltonian $H_{SP} = -\frac{\hbar^2}{2m}\frac{d^2}{dx^2} + V(x)$.

$$\hat{\Psi}(x) = \sum_{j,l} \hat{b}_j^l \psi^l(x - x_j) \,, \tag{2.36}$$

where the subscript $j \in R, L$ is the site index, $x_j \in a/2, -a/2$ are the positions of the minima in the left and right well, the superscript $l \in 0, 1$ is the energy level index, and

$$\begin{aligned} [\hat{b}_j^l, \hat{b}_{j'}^{l'\dagger}] &= \delta_{jj'}\delta_{ll'} \\ [\hat{b}_j^{l\dagger}, \hat{b}_{j'}^{l'\dagger}] &= [\hat{b}_j^l, \hat{b}_{j'}^{l'}] = 0 \,. \end{aligned} \tag{2.37}$$

Generally $\psi^l$ is computed numerically but can be approximated by the eigen-functions of the harmonic oscillator for a sufficiently high barrier $V_0$.

Substituting Eq. 2.36 into 2.34 yields the following two-level Hamiltonian,

$$H = H^0 + H^1 + H^{01}\,, \tag{2.38}$$

where

$$H^l = -J^l \sum_{j \neq j'} \hat{b}_j^{l\dagger} \hat{b}_{j'}^l + U^l \sum_j \hat{n}_j^l (\hat{n}_j^l - 1) + E^l (\hat{n}_R^l + \hat{n}_L^l) \tag{2.39}$$

describes particles on the $l^{th}$ energy level and

$$H^{01} = U^{01} \sum_{j, l \neq l'} (2\hat{n}_j^l \hat{n}_j^{l'} + \hat{b}_j^{l\dagger} \hat{b}_j^{l\dagger} \hat{b}_j^{l'} \hat{b}_j^{l'}) \tag{2.40}$$

couples the energy levels. Here $\hat{n}_j^l = \hat{b}_j^{l\dagger} \hat{b}_j^l$ is the number of particles in the $j^{th}$ site and $l^{th}$ energy level, $E^l$ is the energy of the $l^{th}$ excited state, $J^l$ and $U^l$ are the tunnelling and interaction energies determined by the overlap integrals of the single-particle wave-functions. In the following we set $E^0 = 0$ and the energy between level spacings is defined to be $E^1 - E^0 = \hbar\omega$.

The tunnelling term $J^l$ allows particles to move between wells to the same level. Particles in the same well interact with energy $U^0$ if they are on the same level and $U^{01}$ if they occupy different levels. Interactions between particles in different wells are negligible and have been neglected. Although single-particle tunnelling between levels in a well is forbidden, two particles can hop between energy levels together as described in the 'coupling' Hamiltonian $H^{01}$.

By inspection of Eq. (2.38) we see that in the high barrier limit, $J^0 \ll |U^0|$, the rate at which energy increases as a function of the interaction energy is largely due to how the particles are distributed in each well. The first eigen-value crossing occurs at a particular value of $U^0$ when the maximum of the eigen-values for the first $N+1$ states with no occupation in the excited states coincides with the minimum eigen-value of the states with one particle in the excited level. For a system with an odd number of particles this is calculated to be

$$\begin{aligned} U^0\left[N(N-1)\right] &= \hbar\omega + U^0\left[2\left(\frac{N-1}{2}\right)\left(\frac{N-3}{2}\right)\right] + 4U^{01}\left[\left(\frac{N-1}{2}\right)\right] \\ U^0 &= \frac{2\left(\hbar\omega + 2U^{01}(N-1)\right)}{N^2+2N-3}\,. \end{aligned} \tag{2.41}$$

As expected the same result is found for a system with an even number of particles. Note the divergence at $N = 1$ indicating that there is no eigen-value crossing for a system with a single particle.

In the presence of a high barrier the eigen-states appear as pairs of nearly degenerate antisymmetric (-) and symmetric (+) states,

$$|\Psi_{\pm};\nu\rangle = \frac{1}{\sqrt{2}}\left(|N-\nu,\nu\rangle \pm |\nu,N-\nu\rangle\right) , \tag{2.42}$$

where $0 \leq \nu \leq \frac{N}{2}$. The energy difference between a pair of states is [22]

$$\Delta E_{\nu} = \frac{4U^0\left(\frac{J^0}{2U^0}\right)^{N-2\nu}(N-\nu)!}{\nu![(N-2\nu-1)!]^2} . \tag{2.43}$$

## 2.7 Quantum Sloshing

In chapter 5 we will be investigating quantum sloshing. Quantum sloshing is the tunnelling dynamics of a system of particles in a double well initially localised in either well. In particular we will partially reproduce and extend the work of Carr et. al. using the MCTDH method. To keep this thesis self-contained we summarise the relevant results from [23] below.

The two-mode Hamiltonian for N interacting bosons in a symmetric double well is

$$\hat{H} = -J\sum_{j\neq j'}\hat{b}_j^{\dagger}\hat{b}_{j'} + U\sum_j \hat{n}_j(\hat{n}_j - 1) \tag{2.44}$$

where the subscripts $j$,$j' \in \{R, L\}$ are the indices for the right and left wells, J is the tunnelling energy, U is the interaction energy, $\hat{n}_j = \hat{b}_j^{\dagger}\hat{b}_j$, and both $\hat{b}_j^{\dagger}$ and $\hat{b}_j$ obey the normal creation and annihilation commutation relations.

An arbitrary state vector in Fock space is given by

$$|\Psi\rangle = \sum_{n_L=0}^{N} c_{n_L}|n_L, N-n_L\rangle \; = \sum_{n_L}^{N} c_{n_R}(a_L^{\dagger})^{n_L}(a_R^{\dagger})^{N-n_L}\,|vac\rangle\,, \tag{2.45}$$

where $n_L$ is the number of particles in the left well and $a_i$, $i \in \{R, L\}$ are the creation operators for a particle in the right or left well. For the purposes of the discussion below we consider all particles prepared in the left well, that is $|\Psi(t=0)\rangle = |N, 0\rangle$. The dynamics of the system at a later time, $t$, are described by $|\Psi(t)\rangle = e^{-iHt}|\Psi\rangle$ and the probability of finding $n_L$ particles in the left well at

some time $t > 0$ is $P_{n_L}(t) = |\langle n_L, N - n_L|\Psi(t)\rangle|^2$.

### 2.7.1 Uncorrelated Regime

We first consider N non-interacting bosons ($U = 0$).The lowest lying spectrum of $N$ bosons is found by distributing all atoms over the symmetric and anti-symmetric single-particle orbital of the lowest doublet. These $N + 1$ states

$$|\phi_k\rangle = \left(a_L^\dagger + a_R^\dagger\right)^{N-k} \left(a_L^\dagger - a_R^\dagger\right)^k |vac\rangle \tag{2.46}$$

satisfy $H|\phi_k\rangle = E_k|\phi_k\rangle$ where

$$E_k = N\varepsilon_0 + k\Delta E\,. \tag{2.47}$$

Here $\Delta E = \varepsilon_1 - \varepsilon_0$ is the energy difference between these two orbitals. The eigenvalues of the single particle Hamiltonian

$$H_S = \begin{pmatrix} \varepsilon_L & J \\ J & \varepsilon_R \end{pmatrix}\,, \quad \text{where } \varepsilon_L = \varepsilon_R = \varepsilon \tag{2.48}$$

are explicitly $\varepsilon_0 = \varepsilon - J$ and $\varepsilon_1 = \varepsilon + J$. Thus we find a relationship between $\Delta E$ and $J$, that is $J = \Delta E/2$.

We consider the dynamics of the system where initially all particles occupy the left well, that is $|\Psi(t = 0)\rangle = (a_L^\dagger)^N|vac\rangle$. To see how the initial state evolves in time we look at the time-dependent single-particle creation operator $a^\dagger(t) = a_L^\dagger f(t) + a_R^\dagger g(t)$ in the Heisenberg picture,

$$\begin{aligned} \frac{ida^\dagger}{dt} &= -[H, a^\dagger(t)] \\ &= J\left[(a_L^\dagger a_R + a_R^\dagger a_L)a^\dagger(t) - a^\dagger(t)(a_L^\dagger a_R + a_R^\dagger a_L)\right] \\ &= J\left[a_R^\dagger f(t) + a_L^\dagger g(t)\right]\,. \end{aligned} \tag{2.49}$$

We are left to solve the coupled differential equations

$$\begin{aligned} f'(t) &= -\frac{i\Delta E}{2} g(t) \\ g'(t) &= -\frac{i\Delta E}{2} f(t)\,, \end{aligned} \tag{2.50}$$

with initial conditions $f(0) = 1$ and $g(0) = 0$. The general solutions are given by

$$\begin{aligned} f(t) &= A\cos(Jt) + iB\sin(Jt) \\ g(t) &= C\cos(Jt) + iD\sin(Jt)\,. \end{aligned} \tag{2.51}$$

Upon use of the initial conditions and $\sqrt{|A|^2+|B|^2} = \sqrt{|C|^2+|D|^2} = 1$, due to having a single particle, we find

$$\begin{aligned} f(t) &= \cos(Jt) \\ g(t) &= e^{i\theta}\sin(Jt)\,, \end{aligned} \tag{2.52}$$

where $e^{i\theta} = -1$ is a phase factor determined by Eq. (2.50). The time evolved ket is rewritten

$$|\Psi(t)\rangle \;=\; (a^\dagger(t))^N|vac\rangle \;=\; \frac{1}{\sqrt{N!}2^{N/2}}\left[a_L^\dagger\cos(Jt) - a_R^\dagger\sin(Jt)\right]^N|vac\rangle\,. \tag{2.53}$$

With this result we study some of the characteristics of the system. The probability of finding all particles in the left well is

$$\begin{aligned} P_0(t) &= \left|\langle N,0|\Psi(t)\rangle\right|^2 \\ &= \left|\frac{1}{2^{N/2}\sqrt{N!}}\langle N,0|\left[a_L^\dagger\cos(Jt) - a_R^\dagger\sin(Jt)\right]^N|vac\rangle\right|^2 \\ &= cos^{2N}(Jt)\,, \end{aligned} \tag{2.54}$$

which agrees with [23] (for the alternative method used by [24] see appendix). Thus we find that the particles travel sinusoidally between wells with a period of $T = \pi/J$ which does not depend on N. By a similar, but longer argument (see appendix) we find that the number of particles occupying the left well at any time $t$ is

$$n_L(t) \;=\; \langle\Psi(t)|a_L^\dagger a_L|\Psi(t)\rangle \;=\; N\cos^2(Jt)\,. \tag{2.55}$$

### 2.7.2 Interacting Bosons

We now look at interacting bosons meeting the condition $J \ll |U|$ which is necessary for the creation of MS states. The two highest excited states are symmetric and antisymmetric NOON states, written $|\pm\rangle = \frac{1}{\sqrt{2}}(|N,0\rangle \pm |0,N\rangle)$ and associated with the eigen-values $\varepsilon$ and $\varepsilon + \Delta E$. The energy difference $\Delta E$ between these two

states was given in the last section

$$\Delta E = \frac{4U\left(\frac{J}{2U}\right)^N N!}{[(N-1)!]^2} \tag{2.56}$$

The initial state, $|\Psi(0)\rangle = \frac{1}{\sqrt{2}}(|+\rangle - |-\rangle)$, is a superposition of the (anti-)symmetric eigen-states and thus evolves in time as follows,

$$\begin{aligned} e^{-iHt}|0,N\rangle &= \frac{1}{\sqrt{2}}\left(e^{-i\varepsilon t}|+\rangle - e^{-i(\varepsilon+\Delta E)t}|-\rangle\right) \\ &= -e^{\frac{-i(\varepsilon+\Delta E)t}{2}}\left(\cos(\frac{\Delta E t}{2})|0,N\rangle - i\sin(\frac{\Delta E t}{2})|N,0\rangle\right), \end{aligned} \tag{2.57}$$

where $-e^{-i(\varepsilon+\Delta E)t/2}$ is the global phase and can be ignored. The tunnelling period is $T = 4\pi/\Delta E$, because $\Delta E$ is small, $T$ is large, and by Eq. (2.56) becomes larger with increasing $U$.

Chapter 3

# Setup and Rescaling

The purpose of this thesis is to study the few-body dynamics of interacting one-dimensional Bose gases. We have already seen in the limit where $g \to \infty$ the system of bosons may be mapped to an ideal Fermi gas. In this chapter we will explore this further and in particular investigate how to reproduce the exact eigen-values in this regime in a truncated Hilbert space.

## 3.1 Setup

Before we begin calculations with MCTDH we briefly discuss how it solves the Hamiltonian and decide what parameters should be used to minimise numerical inaccuracies. Also a scaling scheme is introduced to do away with dimensionful parameters.

### 3.1.1 Choosing Parameters

We have already seen that the Hamiltonian describing $N$ non-interacting bosons of mass $m$ in a quasi-1D trap may be written as

$$H = \sum_{i=1}^{N} h(p_i, x_i) + \sum_{i<j} V(x_i - x_j)\,, \tag{3.1}$$

where $h(p,x) = \frac{1}{2m}p^2 + U(x)$ is the single-particle Hamiltonian and $V(x_i - x_j) = g\delta(x)$ is the effective two-body interaction potential. To solve this MCTDH discretizes space using discrete variable representation [20]. However, implementing

the delta function is problematic because it introduces discontinuities. For this reason $\delta(x)$ is replaced with a Gaussian

$$\delta_\sigma(x) = \frac{1}{\sqrt{2\pi\sigma}} e^{-x^2/2\sigma^2}\,, \tag{3.2}$$

which converges to $\delta(x)$ if $\sigma$ is smaller than the 1D scattering length. To limit numerical inaccuracies incurred by making this approximation we impose the following constraints on $\sigma$. We require it to be short-ranged compared to the average inter-particle distance, that is $\sigma \ll L/N$, where $L$ is the systems spatial extension - in our case $L = 2 \times 5$ (i.e. $-5 \leq x \leq 5$). Also $\sigma$ must be chosen to be on the same order as the grid spacing $\Delta_g$ in order that the potential $V$ be properly sampled. After setting the number of grid-points $N_g = L/\Delta_g$ to 128, we find $\sigma = 0.05$ a suitable choice for use in all subsequent work.

## 3.2 External Potentials

In this chapter we begin with benchmarking calculations by considering $N$ interacting bosons confined to a well-understood potential - the harmonic oscillator.

$$U(x) = \frac{1}{2}x^2 \tag{3.3}$$

In chapters 4 and 5 we move on and consider the somewhat more interesting double-well potential. A lot of work has already been done on understanding properties of few-body systems in the double well using approximate techniques such as the Bose-Hubbard model [23]. Furthermore in his thesis [25] Zöllner uses the MCTDH approach to study atoms in a double well modelled by $U(x) = 1/2x^2 + h\delta_w(x)$, a harmonic oscillator plus Gaussian potential. This thesis seeks to reproduce and extend this work by considering $N$ bosons in the Duffing double-well potential

$$U(x) = h(x^2 - x_0^2)^2\,. \tag{3.4}$$

Here is a double well with a barrier height of $U(0) = hx_0^4$, which separates the left and right wells whose minima lie at $\mp x_0$ respectively. The height of the barrier controls tunnelling between wells, where in the limit $h \to \infty$ we are left with two isolated wells.

### 3.2.1 Scaling

For the sake of generality the Hamiltonian is rescaled to the length of the 1D longitudinal system ($a_\parallel = \sqrt{\hbar/M\omega_\parallel}$) or half the distance between the minima of the left and right wells ($a_\parallel = x_0$). This depends on whether the system is confined to a single- or double-well potential respectively. The energy scale $\hbar\omega_\parallel$ in the case of the harmonic potential depends on the trapping frequency $\omega_\parallel$. The double well $\hbar\omega_\parallel$ is defined quite differently as discussed in Sec. 4.1. We rescale then by applying a global coordinate transformation $\mathbf{X}' := \mathbf{X}/a_\parallel$ with $\mathbf{X} \equiv (x_1, \ldots x_N)^T$ such that $H$ becomes

$$H'(\mathbf{X}') = \sum_{i=1}^{N} \left( -\frac{1}{2}\partial_i'^2 + U'(x_i') \right) + \sum_{i<j} V'(x_i' - x_j') \; . \tag{3.5}$$

Thus we are left with a Hamiltonian devoid of physical units. Each quantity is related to the corresponding dimensionless quantity via the following transformations,

$$\begin{aligned} \tilde{x} &:= \frac{x}{a_\parallel} \\ \tilde{U} &:= \frac{U}{\hbar\omega_\parallel} \\ \tilde{g} &:= \frac{g}{\hbar\omega_\parallel a_\parallel} \\ \tilde{t} &:= \omega_\parallel t \end{aligned} \tag{3.6}$$

In the interest of clarity the primes and $\parallel$ subscripts are omitted from here on.

## 3.3 MCTDH and High Correlations

Solving the many-body problem is difficult, and in the case of strong interactions the only method is numerical diagonilization of the many-body Hamiltonian [26]. We have already seen that $g = 0$ and $g \to \infty$ provide two soluble regimes which may be used for calibrating MCTDH. With this in mind we will follow three atoms as they move from the non-interacting regime through to a Tonks-Girardeau gas.

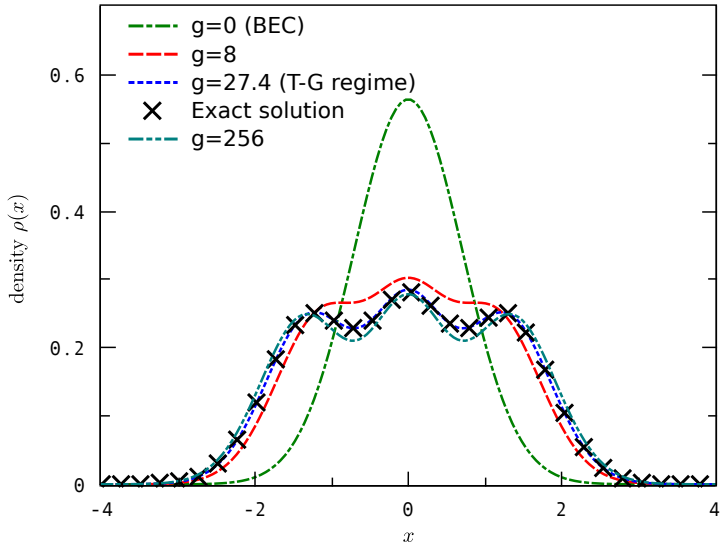


Figure 3.1: Fermionization of bosons in the harmonic potential: The density profile of three bosons at several interactions ($g$). Note that for $g > 27.4$, MCTDH no longer produces a physical result seen by the density profile falling below the exact solution. (15 SPFs)

### 3.3.1 Density Profile

We consider the characteristics of this crossover by looking at the density profile $\rho_B(x)$ (Fig. 3.1), which is the probability of finding a boson at $x$. At $g$ near 0 all particles reside in the groundstate of the harmonic potential, $|\Psi_B\rangle = 1/\sqrt{N!}[a_0^\dagger]^N|vac\rangle$. As $g$ increases we see that the density profile changes significantly by broadening and developing into three peaks. This makes sense intuitively, for three highly interacting bosons will distribute themselves in a manner that pays the least interaction energy.

The ground-state fermionic wave-function is the product of single particle orbitals, that is $|\Psi_F\rangle = \prod_{i=0}^{N-1} a_i^\dagger|vac\rangle$. For $N$ fermions this means

$$\begin{aligned}\rho_F(x) &= \langle\Psi_F|\hat{\Psi}^\dagger\hat{\Psi}|\Psi_F\rangle \\ &= \sum_{j=0}^{N-1} n_j|\phi_j|^2\langle vac|\prod_{i=0}^{N-1} a_i a_i^\dagger|vac\rangle \\ &= \sum_{j=0}^{N-1}|\phi_j|^2\,, \end{aligned} \tag{3.7}$$

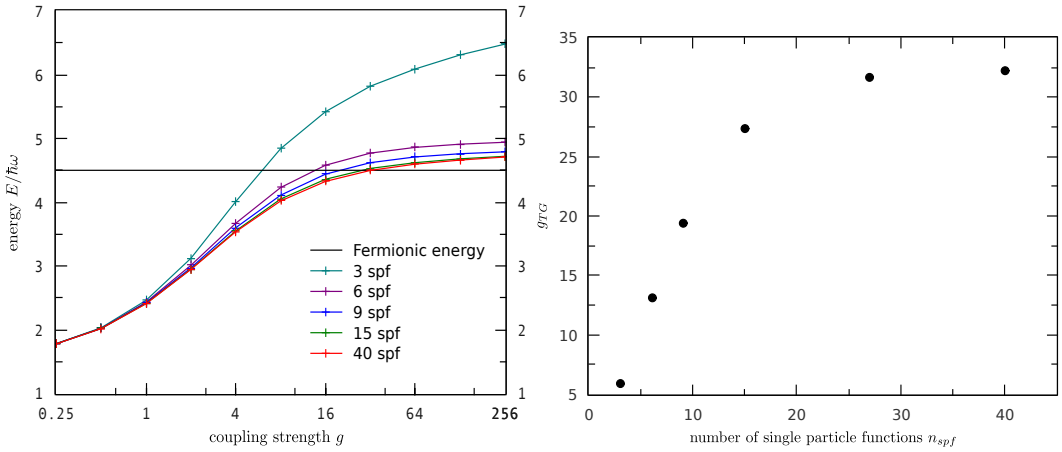


(a) (b)

Figure 3.2: Three bosons in a harmonic trap: (a) The ground-state energy $E(g)$ as a function of the coupling strength ($g$) using different numbers of SPFs. (b) Coupling strength where simulations reach the T-G limit as a function of $n_{spf}$. Theoretically we only approach the fermionic limit as $g \to \infty$. However, we see that this is only the case when $n_{spf} \to \infty$.

where

$$\hat{\Psi}(x) = \sum_j a_j \phi_j(x) \tag{3.8}$$

is the field operator which annihilates a particle at coordinate $x$, $\phi_i(x)$ is the $i^{th}$ single particle function of the harmonic potential, and Eq. (3.7) holds because $n_i = 1 \; \forall \, i$. In the Tonks-Girardeau regime $\rho_B(x) = \rho_F(x)$. However, we find that at $g = 27.4$, far before expected, we already have the density profile of an ideal Fermi gas. This of course results from truncating the Hilbert space. The next couple of sections look at how this can be improved.

### 3.3.2 Single-Particle Functions

The first and most obvious way of improving results is by enlarging the Hilbert space, that is increasing the number of single-particle functions ($n_{\mathrm{spf}}$). For weak interactions three bosons can be described very well with only one SPF as noted in the previous section. This means that results agree closely in this range independent of the number of SPFs used (Fig. 3.2a).

We can clearly see that in the strongly correlated regime the systems energy reaches the Tonks-Girardeau limit at some $g_{\mathrm{TG}}$ far below the theoretical prediction. By increasing $n_{\mathrm{spf}}$ we can improve numerical results. By how much they are

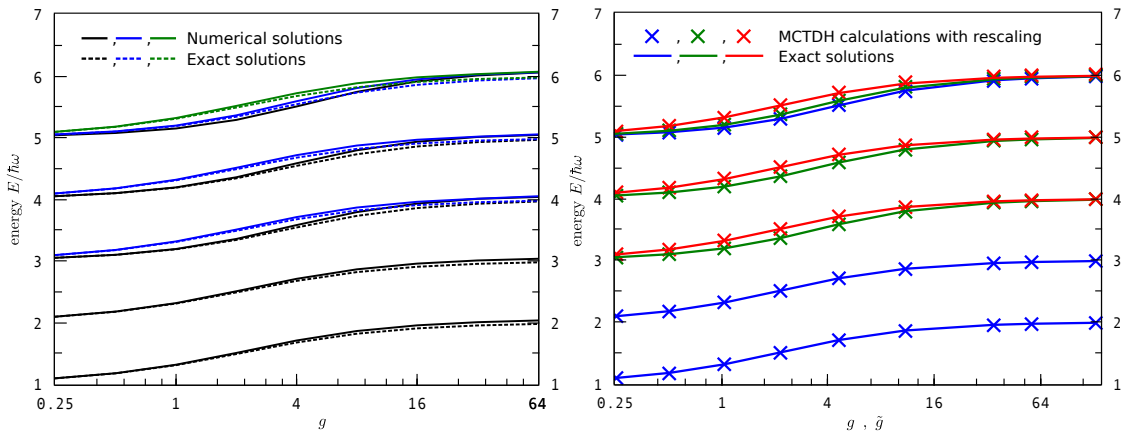


Figure 3.3: Comparing MCTDH with exact two particle model: Plots show energy $E(g)$ of the first nine eigen-states for two bosons in a harmonic trap as a function of the coupling strength. (a) Compares numerical results with the exact results. (b) Compares the rescaled numerical results with exact results. (15 SPFs)

improved is shown in Fig. 3.2b. Although initially the number of SPFs has a large effect on $g_{TG}$ we find that for $n_{\text{spf}} \gtrsim 25$ merely adding more SPFs is ineffectual and in fact paralysing because it becomes more and more computationally expensive. The desire for numerical accuracy at reasonable numbers of SPFs necessitates the use of rescaling introduced in the next section.

## 3.4 Rescaling

The problem of describing atoms in highly-correlated regimes is a difficult one and, as we saw above, simply increasing the Hilbert space does not offer a true solution. The Lee-Suzuki method [27] solves this problem by obtaining effective operators within a reduced basis space. This has been applied to harmonically-confined bosons with good results [28]. Here we present a method which is simpler and only requires knowledge of $g_{\text{TG}}$.

As a test bed for our scheme we return to the system of two interacting bosons, for which an analytical solution exists (see chapter 2). The analytical (a) eigen-values of the two-particle Hamiltonian $H = H_R + H_r$ are $E^a_k(g) = E^R_i + E^r_{2j}(g)$. Here only the even eigen-states of $H_r$ are considered because we are dealing with bosons. We plot the numerical (n) eigen-values $E^n_k$ from $g = 0$ through to a highly correlated regime for the first nine eigen-states and compare with the analytical

results (Fig. 3.3a). Consider for a moment the numerical ground-state energy $E_0^n(g)$. Energy higher than $E_0^n(g_{\mathrm{TG}})$ is physically impossible, which clearly shows that there is a discrepancy between the numerical and analytical results. Hallwood et. al. [29] has developed an effective Hamiltonian by rescaling $g$ to recover the exact eigen-values for two bosons in a ring. Inspired by its success we implement the following rescaling scheme,

$$\tilde{g} = \frac{g}{1 - g/g_{\mathrm{TG}}}\,, \tag{3.9}$$

which essentially disregards energy values larger than $E_0^n(g_{\mathrm{TG}})$ and introduces $\tilde{g}$. This is done such that $E_0^n \to E_0^n(g_{\mathrm{TG}})$ only as $\tilde{g} \to \infty$. In fact, because all eigen-states reach the Tonks-Girardeau limit at $g_{\mathrm{TG}}$ calculated for the ground-state, we can recycle Eq. (3.9) for use in any of the first nine eigen-states (Fig. 3.3b). This property becomes important when dealing with dynamics.

## 3.5 Summary

As soon as interactions are added to a system of particles the problem of describing it becomes harder. To test MCTDH's capabilities we ran calculations in the harmonic potential. What we found was that merely using more SPFs is not a practical solution to improving numerical inaccuracies, which are seen especially in the highly-correlated regimes. However, by rescaling $g$ we obtain an effective Hamiltonian inside the truncated Hilbert space which recovers the exact eigen-values. Results from recycling this rescaling scheme to higher eigen-states suggest useful application of this effective Hamiltonian to dynamical systems. In the next two chapters we study few-body systems in the double-well, but because we are only interested in effects well below the fermionic limit this rescaling is not used in subsequent work.

Chapter 4

# MCTDH and the Eigen-Value Crossings

So far we have seen MCTDH in action but have only applied it to a simple and well-understood system. We will now study the features of interacting bosons in a double well. This chapter concerns itself with the interplay between the coupling strength and the barrier separating the two wells. In particular we are interested to see if MCTDH has any advantages over the 4-mode Bose-Hubbard model.

## 4.1 Single-Particle Spectrum

To understand some key features of the double well we turn to the single-particle spectrum. The first thing noticed in Fig. 4.1 is that the single-particle spectrum has a doublet structure. Being well separated by the barrier the lowest lying doublets, $i = 0, 1, \ldots, k$ ($k$ dependent on $h$), are anti-symmetric (-) and symmetric (+) orbitals of the form $\phi_i^{\pm}(x) = 1/\sqrt{2}[w_i(x + x_0) \pm w_i(x - x_0)]$, where $w_i$ is some localised function and $H|\phi_i^{\pm}(x)\rangle = \varepsilon_i^{\pm}|\phi_i^{\pm}(x)\rangle$. A doublet is separated in energy by the tunnel splitting $\Delta\varepsilon_i = \varepsilon_i^- - \varepsilon_i^+$, which is much smaller than the inter-level spacing $\Delta E_i = \varepsilon_{i+1}^+ - \varepsilon_i^-$. We define $\hbar\omega = \Delta E_0 = \varepsilon_1^+ - \varepsilon_0^-$.

## 4.2 Energy Spectrum

In this section we discuss how the energy of a 1D Bose gas is expected to change in its crossover from the uncorrelated regime to the Tonks-Girardeau limit. In

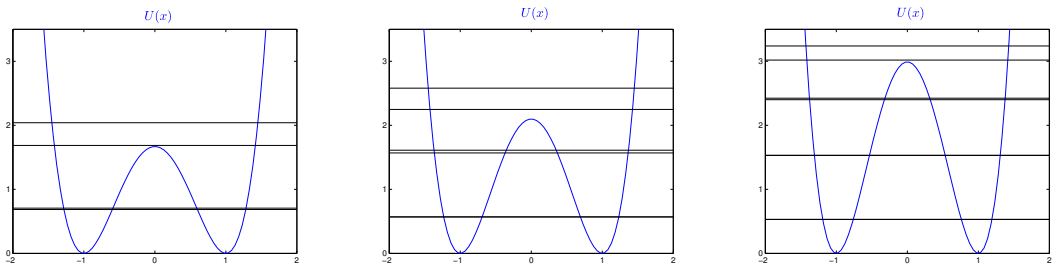


(a) (b) (c)

Figure 4.1: Single particle spectrum $\{\varepsilon_i\}$ in a duffing double well with barrier height (a) $h = 1.67\hbar\omega$, (b) $h = 2.09\hbar\omega$, and (c) $h = 2.97\hbar\omega$.

the uncorrelated regime, $g = 0$, all $N$ particles are simply distributed over the single-particle states. Finding the total energy involves adding the corresponding eigen-values

$$E = \sum_{s=\pm} \sum_{i} A_i^s \varepsilon_i^s \,, \tag{4.1}$$

where $A_i^{\pm} \in \{0, 1, \ldots, N\}$ and $\sum_{s=\pm} \sum_i A_i^s = N$. In the Tonks-Girardeau limit, $g \to \infty$, the bosonic system undergoes fermionization and

$$E = \sum_{s=\pm} \sum_{i} B_i^s \varepsilon_i^s \,, \tag{4.2}$$

where $B_i^{\pm} \in \{0, 1\}$ and $\sum_{s=\pm} \sum_i B_i^s = N$.

Between these two regimes we make some observations. An arbitrary vector in Fock space is given by

$$\begin{aligned} |\Psi\rangle &= \sum_{\mathbf{n}} C_{\mathbf{n}} |\mathbf{n}\rangle \\ |\mathbf{n}\rangle &\equiv |n_{L_0}, n_{R_0}, n_{L_1}, n_{R_1}, \ldots, n_{L_f}, n_{R_f}\rangle \\ &= \frac{1}{\sqrt{n_{L_0}! n_{R_0}! \cdots n_{L_f}! n_{R_f}!}} [a_{L_0}]^{n_{L_0}} [a_{R_0}]^{n_{R_0}} \cdots [a_{L_f}]^{n_{L_f}} [a_{R_f}]^{n_{R_f}} |vac\rangle \,, \end{aligned} \tag{4.3}$$

where $n_{L_i}$ and $n_{R_i}$ are the number of particles in the $i^{th}$ excited level of the left and right well respectively, and $\sum_{i=0}^{f} (n_{L_i} + n_{R_i}) = N$. Consider the lowest cluster of eigen-states. In the non-interacting regime these $N + 1$ states are the set of states with no occupation in the excited levels, that is $|\Psi\rangle = \sum_{n_{L_0}} C_{n_{L_0}} |n_{L_0}, N - n_{L_0}\rangle$. Of these the highest lying states are quickly characterised by $|\Psi^{\pm}\rangle = |N, 0\rangle \pm |0, N\rangle$, whose energy increases rapidly with increasing $g$ because all particles are localised

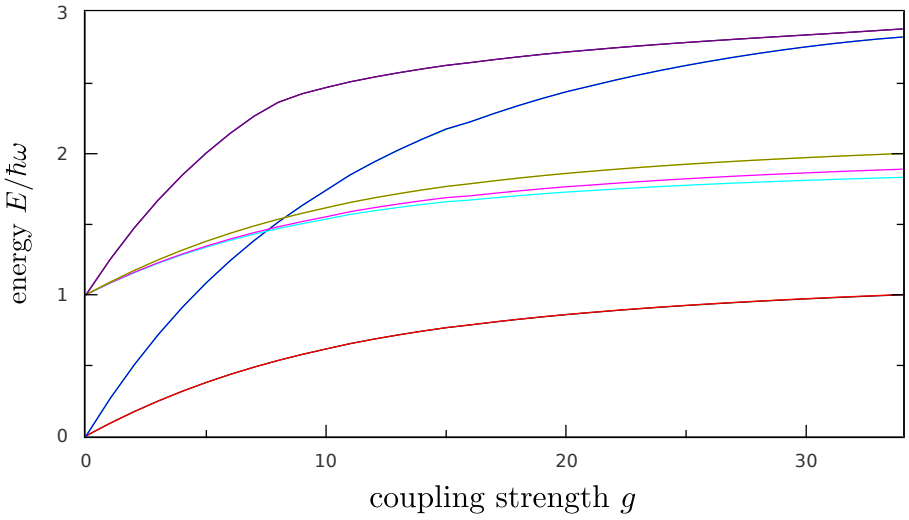


Figure 4.2: Energy spectrum of 3 bosons in a double well of height $h = 2.75\hbar\omega$ as they crossover from the non-interacting regime into the highly correlated regime. Note that the lowest two lines are both nearly degenerate pairs of lines. (20 SPFs for $g \leq 20$, 30 SPFs for $g > 20$, $\hbar\omega = 18.22$)

to one well. On the other hand the lowest lying states are well characterised by $|\Psi^{\pm}\rangle = |\frac{N+1}{2}, \frac{N-1}{2}\rangle \pm |\frac{N-1}{2}, \frac{N+1}{2}\rangle$ (odd $N$) or $|\Psi\rangle = |\frac{N}{2}, \frac{N}{2}\rangle$ (even $N$), whose energy only increases steadily because the particles have a more even distribution. As the system moves into a highly-correlated regime the bosons try to isolate each other so as to pay less interaction energy. Initially this is done with all atoms sharing the same level. However, with sufficient repulsive interactions the bosons redistribute themselves in the manner of spinless fermions. Similar features can be found for any given band of eigen-states.

## 4.3 Energy Difference between NOON States

In chapter 2 we reviewed two results of the Bose-Hubbard model, eigen-value crossings and tunnel splitting between anti-symmetric/symmetric pairs. For the remainder of this chapter we will reproduce and compare these results with the MCTDH approach in the case $N = 3$. We are particularly interested in the energy spectrum about the eigen-value crossings. Section 4.2 provides a useful overview of the general behaviour but to fill in some of the gaps we lower the barrier and restrict the

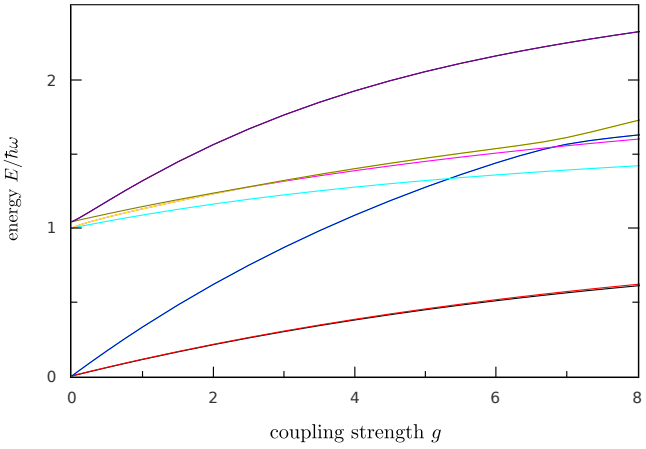


(a)

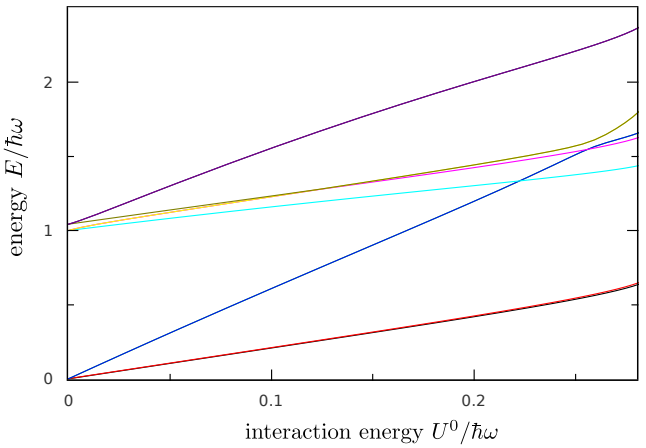


(b)

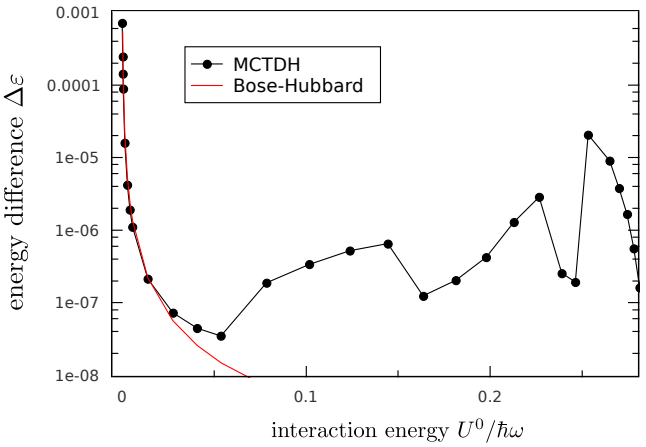


(c)

Figure 4.3: MCTDH vs. two-level Bose-Hubbard: Eigen-values of a 3 boson system in a double-well of height $h = 2.09\hbar\omega$ as a function of (a) The coupling strength ($g$), and (b) The interaction energy ($U^0$). By rescaling $g$ to $U^0$ we can make a direct comparison between MCTDH and Bose-Hubbard. (c) Energy difference between the symmetric and anti-symmetric NOON states as calculated by each method, over $U^0$. We see that MCTDH only agrees with Bose-Hubbard in the weakly-correlated regime. (40 SPFs, $\hbar\omega = 11.92$)

range of $g$ (Fig. 4.3a). Apart from exhibiting the general characteristics of a double-well system, immediately apparent is the avoided crossing at $g \approx 7$. This suggests coupling between the $|N,0\rangle \pm |0,N\rangle$ and $|2,0,0,1\rangle \pm |0,2,1,0\rangle$ states.

The effect of this coupling is demonstrated by considering the energy difference between the anti-symmetric and symmetric NOON states, which for the two-level Bose-Hubbard model is given by Eq. (2.43)

$$\Delta\varepsilon = \frac{3(J^0)^3}{8(U^0)^2} \tag{4.4}$$

However, to make a meaningful comparison with MCTDH the interaction strength $g$ must be rescaled into units of $U^0/\hbar\omega$. A relationship between $g$ and $U^0/\hbar\omega$ is found by using graphing software to fit a second order polynomial $(ag^2 + bg + c)$ to the $(N+1)^{th}$ state in Fig. 4.3a. The gradient of the corresponding state in the Bose-Hubbard model is $N(N-1)U^0 = 6U^0$. Thus we find $U^0 \approx (ag^2 + bg + c)/6$ which upon setting $a = -0.17$, $b = 0.34$, and $c = 0$ produces Fig. 4.3b.

For very weak interactions we see in Fig. 4.3c that the energy difference found using the MCTDH approach ($\Delta\varepsilon^{MCTDH}$) agrees well with Eq. (4.4). However, as $U^0$ increases, $\Delta\varepsilon^{MCTDH}$ diverges from $\Delta\varepsilon$ and is soon characterised by two peaks which centre at the eigen-value crossings, that is, this coupling to higher eigenstates effectively pulls the symmetric and anti-symmetric NOON states apart.

## 4.4 Eigen-Value Crossing

Recall that in the high barrier limit $J^0 \ll U^0$ of the two level Bose-Hubbard model the first eigen-value crossing occurs at some critical value of $U^0$ ($U^0_{crit}$), where

$$U^0_{crit} = \frac{2\left(\hbar\omega + 2U^{01}(N-1)\right)}{N^2 + 2N - 3}\,. \tag{4.5}$$

The derivation of Eq. (4.5) assumes there is no tunnelling between wells, that is $J^0 = 0$. What we expect then for $N = 3$ bosons with the approximation $U^{01} = (1/2)U^0$ [22] is $U^0_{crit} = 0.25\hbar\omega$. We cannot check this prediction with the MCTDH approach in the extreme case above (which is equivalent to $h \to \infty$) but find the effect of raising and lowering the barrier.

We have already seen that values of $h \gtrsim 2\hbar\omega$ are necessary to maintain a NOON state at the first crossing. Fig. 4.4 shows that as the barrier is raised the amount of interaction energy needed to reach $U^0_{crit}$ increases and begins to converge to a value

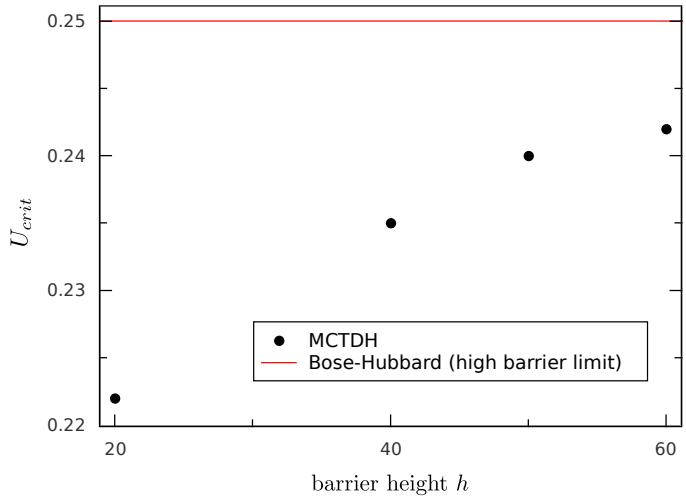


Figure 4.4: Interaction energy needed to reach the first eigen-value crossing ($U^0_{crit}$) as a function of the barrier height $h$. As $h$ increases $U^0_{crit}$ begins to converge to $0.25\hbar\omega$, the value predicted by the Bose-Hubbard model.

near $0.25\hbar\omega$. Thus we observe the first crossing earlier by lowering the barrier and find that the two-level prediction agrees well with MCTDH for large $h$.

## 4.5 Summary

We have seen in chapter 2 that the two-level Bose-Hubbard model can be effectively used to predict characteristics of particles confined to a double-well potential. Here, we have proposed a way to rescale MCTDH's interaction strength ($g$) to the interaction energy ($U^0$) of the Bose-Hubbard model. This allows us to directly compare results between the two methods. We have found two results in particular. When looking at the energy difference ($\Delta\varepsilon$) between NOON states we found that although MCTDH agrees with Bose-Hubbard for small interactions, results differ wildly for $U^0$ around the eigen-value crossings. MCTDH marks the coupling between crossed states by sharp peaks in $\Delta\varepsilon$. We also saw that by raising the barrier ($h$), the first eigen-value crossing found by MCTDH comes into closer agreement with the two-level Bose-Hubbard model. Thus far we have only studied static systems, but we will see that this puts us in good stead to investigate dynamical systems in the double well.

Chapter 5

# Quantum Sloshing

So far we have studied the influence of correlations in a one-dimensional bosonic system. In this chapter we see the physics from the last chapter in the dynamics of $N$ bosons confined to the double well. A particularly interesting quantum phenomenon observed in the double well is tunnelling and ultra-cold atoms provide the means to study it with a high degree of accuracy. By initially preparing all atoms in one well we find for which regimes all atoms tunnel coherently between wells, an effect known as quantum sloshing.

## 5.1 Overview

We will be investigating the time dynamics of three bosons in a symmetric double well as we pass from the uncorrelated regime ($g = 0$) into the weakly correlated regime. The double well ($U(x) = h(x^2 - 1)^2 + lx$) is the quartic plus cubic from the last chapter but generalized to include a linear term. The barrier height ($h = 1.67\hbar\omega$) is carefully chosen. While $U(x)$ must be able to support MS states ($h > E_0$) up to the required interaction strength, the barrier height $h$ should be set low enough to achieve oscillations with a period that is numerically feasible (Fig. 5.1).

Depicted in Fig. 5.2 is the strategy for creating the initial state $\Psi(0)$, which in our case means loading all atoms in the left well. Adding a sufficiently large linear term (depending on $N$ and $g$) to $U(x)$ introduces a tilt in the double well. When we let this system relax into the ground state all atoms are localised into a single

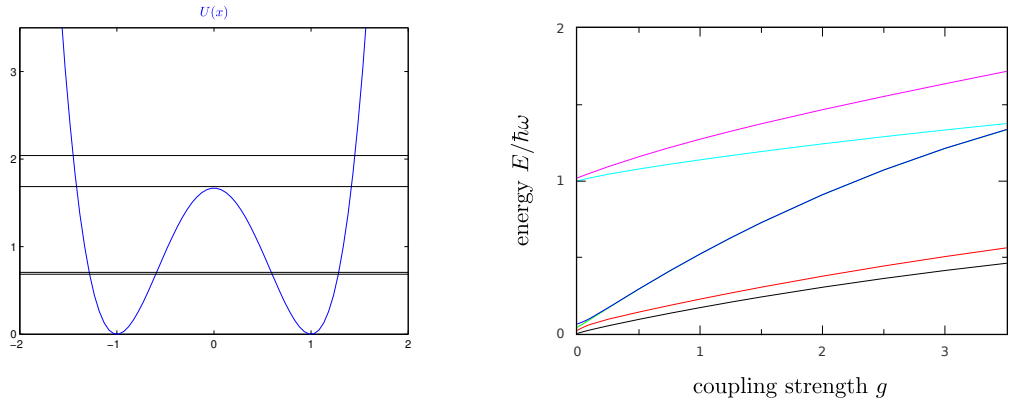


Figure 5.1: (left) Single-particle spectrum of a double well with $h = 1.67\hbar\omega$. (right) Corresponding energy spectrum for three bosons. (40 SPFs, $\hbar\omega = 6$)

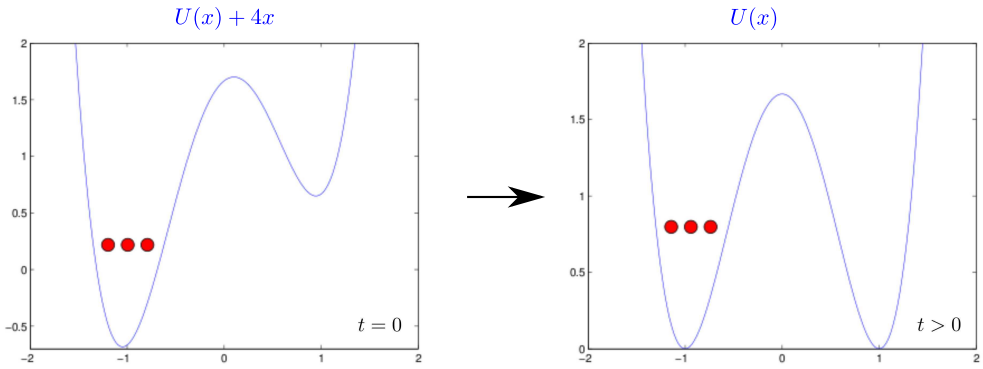


Figure 5.2: Sketch of the setup: At $t = 0$ the system is relaxed into the ground state of a tilted double well (left). The asymmetry is then removed adiabatically leaving all particles initially localised in the left well (right).

well. Before a propagation run the asymmetry is reduced non-adiabatically until we are left with all particles confined into the left well of a symmetric double well.

## 5.2 Results

We consider a system of three bosons initially confined to the left well. Tunnelling between wells is monitored by counting the number of atoms in the left well,

$$n_L(t) = \int_{-\infty}^{0} \rho(x,t)\,\mathrm{d}x\,, \tag{5.1}$$

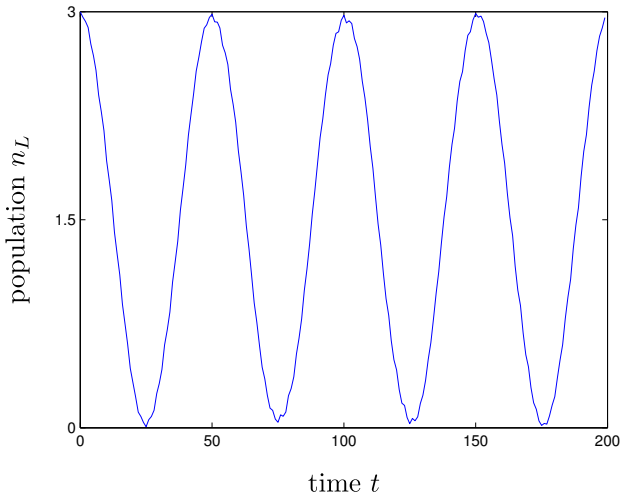


Figure 5.3: Three boson dynamics in the double well of height $h = 1.67\hbar\omega$: Shown is the number of atoms in the left well over time. The 'wobbling' is caused by not adjusting the minimum of the left well in the asymmetric trap to align with the minimum of the left well in the symmetric trap. (20 SPFs)

where $\rho(x,t)$ is the one body density, the probability density for finding a single particle at $x$. In this way the effect of increasing interactions can be investigated.

Although the non-interacting atoms in Fig. 5.3 exhibit quantum sloshing, the behaviour is far from coherent due to the 'wobbling' which is seen particularly when all atoms are localised in the same well. This 'wobbling' is actually oscillations due to the minimum of the left well of the asymmetric potential being shifted to the left of $x = -1$ (seen in Fig. 5.2). It follows that this effect becomes pronounced when all atoms occupy the same well. This is corrected by choosing a suitable value for $d$ such that of the minima found by solving

$$U'(x) = x(x^2 - d^2) + \frac{l}{4h} = 0\,, \tag{5.2}$$

the minimum corresponding to the left well is at $x = -1$. For $l = 4$ this is achieved by setting $d = 0.949$. Once corrected we see the expected coherent oscillations (Fig. 5.4a).

When interactions are turned on the dynamics undergo severe changes. For very weak interactions we observe what appears to be very erratic behaviour (Fig. 5.4b). The dynamics here no longer have just one frequency contribution but many of similar amplitude which compete with each other. Higher interactions are characterised by one frequency modulated by higher frequencies with small amplitude. As

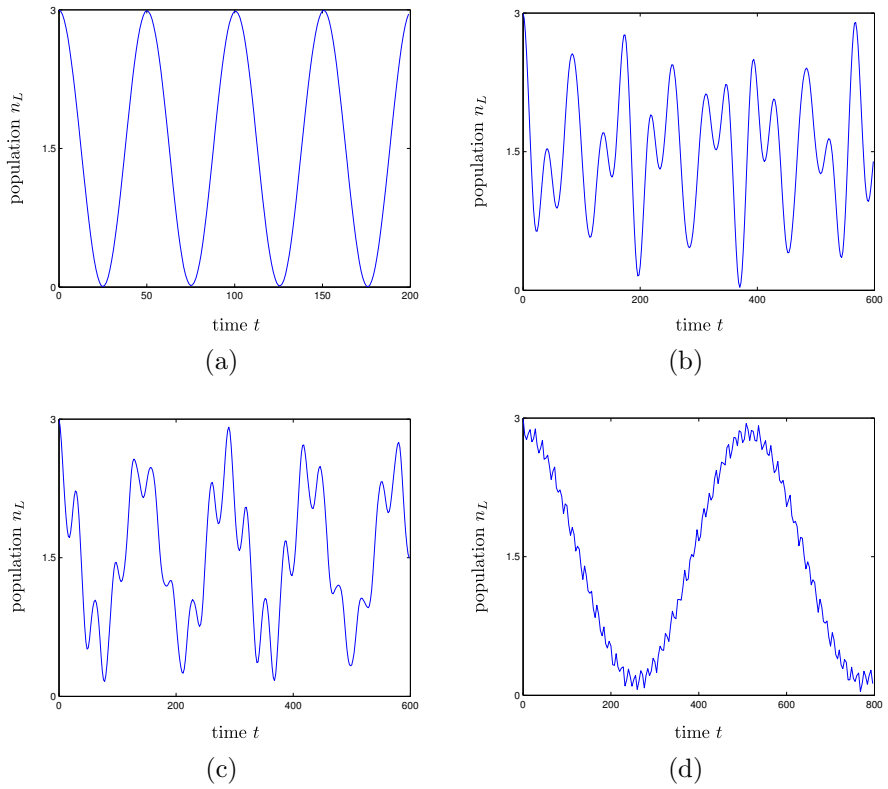


Figure 5.4: Three-boson dynamics in a double well of height $h = 1.67\hbar\omega$: Shown is population in the left well over time, $(n_L(t))$, for (a) $g = 0$, (b) $g = 0.05$, (c) $g = 0.1$, and (d) $g = 0.25$. (20 SPFs)

$g$ continues to increase we see that, somewhat surprisingly, the higher frequencies are all but dampened out and the dynamics again resemble coherent oscillations. The time required for complete population transfer has increased significantly compared with $g = 0$, but because $h = 1.67\hbar\omega$ was carefully chosen we find that the period $T < 900$.

## 5.3 Multi-Mode Analysis

The stark difference in time scales for the coherent oscillations of $g = 0$ and $g = 0.25$ is explained by looking to the evolution of the energy spectrum as it varies over $g$. Here too we can see what causes the seemingly erratic behaviour on the range $0 < g \lesssim 0.25$. The initial many-body wavefunction for $N$ atoms prepared into the left well of the symmetric double well may be written as a superposition of

eigenstates.

$$|\Psi(0)\rangle = \sum_j C_j |\psi_j\rangle \,, \tag{5.3}$$

where $H|\psi_j\rangle = E_j|\psi_j\rangle$. Here the many-body eigenstate $|\psi_j\rangle$ is the linear combination of all possible configurations, that is,

$$\begin{aligned} |\psi_j\rangle &= \sum_{\mathbf{n}} D_{\mathbf{n}} |\mathbf{n}\rangle \\ |\mathbf{n}\rangle &\equiv |n_1, n_2, \ldots, n_M\rangle \\ &= \frac{1}{\sqrt{n_1! n_2! \cdots n_M!}} [a_1^\dagger]^{n_1} [a_2^\dagger]^{n_2} \cdots [a_M^\dagger]^{n_M} |vac\rangle \,. \end{aligned} \tag{5.4}$$

The occupation numbers $n_k$ count the number of particles in the $k^{th}$ single particle function ($\phi_k(x)$) and satisfy conservation of particle number, $\sum_{k=1}^{M} n_k = N$. The initial wavefunction evolves in time as

$$|\Psi(t)\rangle = \sum_j C_j e^{-iE_j t} |\psi_j\rangle \,. \tag{5.5}$$

We make use of Eq. (5.1) to make a direct comparison with results

$$\begin{aligned} n_L(t) &= \int_{-\infty}^{0} \mathrm{d}x \, \rho(x,t) \\ &= \sum_{j,k} C_j^* C_k e^{-i(E_k - E_j)t} \int_{-\infty}^{0} \mathrm{d}x \, \langle \psi_j | \hat{\Psi}^\dagger(x) \hat{\Psi}(x) | \psi_k \rangle \\ &= \sum_j \left[ \left| C_j \right|^2 \sum_l \langle \psi_j | \hat{a}_l^\dagger \hat{a}_l | \psi_j \rangle \int_{-\infty}^{0} \mathrm{d}x \left| \phi_l(x) \right|^2 \right] + \sum_{j>k} \Bigg[ \Big( C_j^* C_k e^{-i\Delta E_{jk} t} \\ &\quad + C_j C_k^* e^{i\Delta E_{jk} t} \Big) \sum_{l,m} \int_{-\infty}^{0} \mathrm{d}x \, \phi_l^*(x) \phi_m(x) \langle \psi_j | \hat{a}_l^\dagger \hat{a}_m | \psi_k \rangle \Bigg] \\ &= \sum_j \Big[ \alpha \Big] + \sum_{j>k} \Big[ (\beta) \sum_{l,m} \gamma \Big] \end{aligned} \tag{5.6}$$

where

$$\hat{\Psi}(x) = \sum_l a_l \phi_l(x) \,, \tag{5.7}$$

found in the second line, is the field operator which annihilates a particle at coordinate $x$ and $\Delta E_{jk} = E_j - E_k$. We can simplify Eq. (5.6) with the following observations. Since $\phi_k(x)$ are the single particle functions of the symmetric double well they are either symmetric or antisymmetric. As a result the $|\phi_k(x)|^2$ term in $\alpha$

is symmetric. It follows that the integral $\int_{-\infty}^{0} \mathrm{d}x\,|\phi_k(x)|^2 = 1/2\ \forall\, k$ and therefore $\sum_j[\alpha] = 1/2\sum_j \left|C_j\right|^2 \sum_l \langle\psi_j|\hat{a}_l^\dagger \hat{a}_l|\psi_j\rangle = N/2$.

We can prove that the coefficients $C_j$ are real using the following substitutions,

$$C_{\mathbf{n}}^* C_{\mathbf{m}} = A + iB \qquad , \qquad C_{\mathbf{n}} C_{\mathbf{m}}^* = A - iB\,. \tag{5.8}$$

With these identities we find $\beta = 2\Big(A\cos(\Delta E_{jk}t) - B\sin(\Delta E_{jk}t)\Big)$. Essentially the effect of adding $\sin(\Delta E_{jk}t)$ is to add a phase to $\cos(\Delta E_{jk}t)$. However, because all atoms are initially in the left well, $\cos(\Delta E_{jk}t)$ finds maximum amplitude at $t = 0$ which implies that $B = 0$.

The dynamics of the system are governed by the $N(N+1)$ off diagonal terms. However, many of these terms fail to contribute for the following reason. Because $\hat{a_k}$ is a single particle operator then $\langle\psi_j|\hat{a}_l^\dagger \hat{a}_m|\psi_k\rangle$ only couples $|\psi_j\rangle$ with those 'neighbouring' states $|\psi_k\rangle = |\psi_{j+1}\rangle$, where just one particle occupies a different single particle state. With these considerations Eq. (5.6) may now be written as

$$n_L(t) = \frac{N}{2} + 2\sum_j \Big(A_{j,j+1}\cos(\Delta E_{j+1,j}t)\Big) \sum_{l,m} \int_{-\infty}^{0} \mathrm{d}x\,\phi_l^*(x)\phi_m(x)\langle\psi_j|\hat{a}_l^\dagger \hat{a}_m|\psi_{j+1}\rangle\,. \tag{5.9}$$

## 5.4 Analysis of Results

In the analysis that follows we assume that because our system has been carefully prepared the $N = 3$ atoms are restricted to the lowest two modes. We can only solve the integral in Eq. (5.9) analytically for two specific cases, $g = 0$ and the NOON state regime. However this provides us with the tools necessary to explain the behaviour through the range of $g$.

### 5.4.1 Non-Interacting Regime

In the case $g = 0$ the $N + 1 = 4$ states are simply the distribution of the particles over the lowest-lying symmetric and antisymmetric single particle orbitals.

$$|\psi_j\rangle = [a_1^\dagger]^{3-j}[a_2^\dagger]^j|vac\rangle, \qquad j = 0\ldots 3 \tag{5.10}$$

The corresponding eigen-values are $E_j = E_0 + j\Delta E$, where $\Delta E = \varepsilon_1 - \varepsilon_0$ is the energy difference between these two orbitals. Thus in the non-interacting regime

Eq. (5.9) becomes

$$\begin{aligned} n_L(t) &= \frac{3}{2} + \cos(\Delta E t) \underbrace{\sum_{j=0}^{2} 2A_{j(j+1)} \sum_{l,m} \int_{-\infty}^{0} \mathrm{d}x\, \phi_l^*(x)\phi_m(x)\langle\psi_j|\hat{a}_l^\dagger \hat{a}_m|\psi_{j+1}\rangle}_{\equiv\xi} \\ &= \frac{3}{2} + \frac{3}{2}\cos(\Delta E t)\,, \end{aligned} \tag{5.11}$$

where we have made use of the fact that $n_L(0) = 3$ to find $\xi = 3/2$. From this we can conclude that the equidistance of the levels guarantees simple coherent oscillations with a period of $2\pi/\Delta E$.

### 5.4.2 NOON State Regime

Whereas the eigen-states at $g = 0$ are non-localised, for higher interactions they evolve into the superpositions of functions localised in the left and right wells. That is

$$\begin{aligned} |\psi_j\rangle' &= \sum_{\mathbf{n}} D'_{\mathbf{n}} |\mathbf{n}\rangle' \\ |\mathbf{n}\rangle' &\equiv \frac{1}{\sqrt{n_L!(3-n_L)!}} [b_1^\dagger]^{n_L} [b_2^\dagger]^{3-n_L} |vac\rangle\,, \end{aligned} \tag{5.12}$$

where $n_L$ refers to the number of particles in the left well, $b_1^\dagger = 1/\sqrt{2}(a_1^\dagger + a_2^\dagger)$ and $b_2^\dagger = 1/\sqrt{2}(a_1^\dagger - a_2^\dagger)$. We have already seen in chapter 2 that at some $g = g_{\mathrm{NOON}}$ the initial state $|3,0\rangle'$ may be written as the superposition of $|\psi_2\rangle' = |3,0\rangle' + |0,3\rangle'$ and $|\psi_3\rangle' = |3,0\rangle' - |0,3\rangle'$, that is the $3^{rd}$ and $4^{th}$ eigen-states. As a result the dynamics will consist of the population shuffling between $|3,0\rangle'$ and $|0,3\rangle'$. This is further demonstrated by simplifying Eq. (5.9).

$$n_L(t) = \frac{3}{2} + \frac{3}{2}\cos(\Delta E_{32} t)\,. \tag{5.13}$$

Thus when $g \geq g_{\mathrm{NOON}}$ we are said to be in the NOON state regime. We will see coherent oscillations with a period of $2\pi/\Delta E_{32}$.

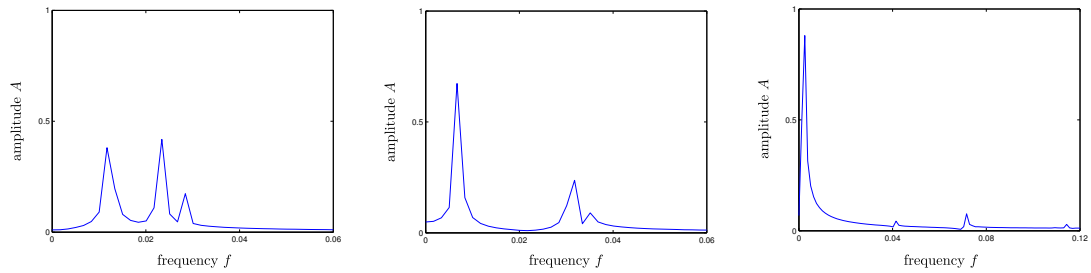


(a) (b) (c)

Figure 5.5: Frequency components of $n_L(t)$ seen in Fig. (a) 5.4b, (b) 5.4c, and (c) 5.4d calculated using the Fourier transform. Sampling times used in the transform are equal to the times reported in the above mentioned figures.

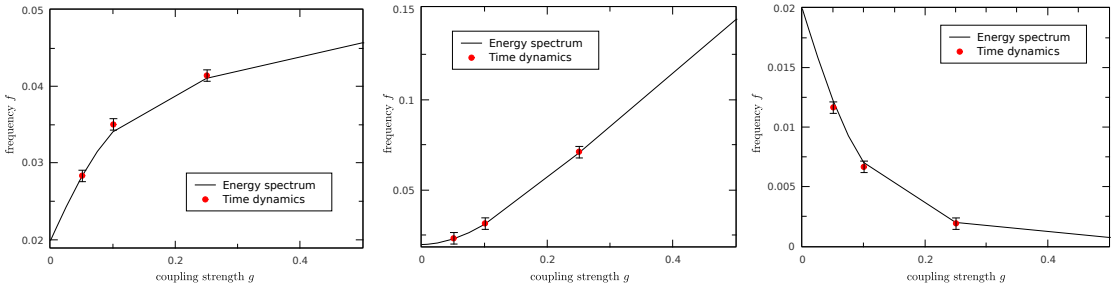


(a) (b) (c)

Figure 5.6: Comparison of the frequency components of $n_L(t)$ calculated from the time dynamics and energy spectrum in the double-well potential: Shown are frequencies corresponding to the (a) ground and $1^{st}$ excited states, (b) $1^{st}$ and $2^{nd}$ excited states, and (c) symmetric and anti-symmetric NOON states. Finite sampling time $t$ introduces errors into the analysis equal to $1/t$.

### 5.4.3 Intermediate Interaction Regime

Given Eqs. (5.11) and (5.13), it would not be unreasonable to assume that on the range $0 < g < g_{\text{NOON}}$ Eq. (5.9) simplifies to

$$n_L(t) = \frac{3}{2} + \frac{3}{2}\sum_j A_{j,j+1}\cos(\Delta E_{j,j+1}t)\,. \tag{5.14}$$

It is difficult to prove this analytically but we may test it numerically by separating the contributing frequencies using the Fourier transform (Fig. 5.5). We note that at small interactions the amplitudes $A_{jk}$ for each of the frequencies are approximately the same. However, as interactions move toward $g_{\text{NOON}}$ the amplitude correspond-

ing to the symmetric and anti-symmetric NOON states ($A_{23}$) begins to dominate. This suggests there is only one contributing frequency in the NOON regime. The frequencies recovered by the Fourier transform, perhaps unsurprisingly, correspond to the energy difference between neighbouring states (Fig. 5.6). Although this means Eq. (5.14) describes the dynamics for any interaction strength, we are left to solve the amplitudes numerically in the range $0 < g < g_{\mathrm{NOON}}$.

## 5.5 Summary

In this chapter we see the relationship between dynamical systems and the time-independent calculations of chapter 4. We find that the dynamics caused by initially preparing all atoms into the left well is described by the energy difference between neighbouring states. This means we find coherent oscillations in the uncorrelated regime because the states are equidistant. Coherent oscillations are also found in the NOON state but this is because only the energy difference between the symmetric and anti-symmetric NOON states contribute.

Chapter 6

# Conclusions

We have studied few-body systems of ultra-cold interacting bosons confined to one-dimensional single- and double-well potentials. We investigated these systems in both weakly- and strongly-correlated regimes. This was done using the multi-configurational time-dependent Hartree (MCTDH) approach.

The problem of accurately describing interacting particles is a difficult one, especially in the highly-correlated regime. In chapter 2 we found that merely enlarging the Hilbert space does not offer a practical solution to improving numerical inaccuracies. For example, in our study of three bosons in the harmonic potential it was found that if more than twenty single-particle functions were used, calculations just become more and more computationally demanding with little improvement in accuracy. In section 3.4 we introduced a rescaling scheme that obtains an effective Hamiltonian inside the truncated Hilbert space which recovers the exact eigen-values. This was applied with good results to the system of two particles in the harmonic trap, for which an exact solution exists. Also we are able to apply the rescaling found for the ground state to higher-lying states. This suggests the method to be of service when considering dynamical systems.

The two-level Bose-Hubbard model has been used effectively in describing the features of bosons in the double-well potential. However, it is only a two-level approximation and so we compare some of its predictions with MCTDH. To make direct comparison we proposed a way to rescale MCTDH's coupling strength ($g$) to the interaction energy ($U^0$) of the Bose-Hubbard model. Thus when looking at the energy difference ($\Delta\varepsilon$) between the symetric and anti-symetric NOON states we find that Bose-Hubbard only agrees with MCTDH in the weakly-correlated regime.

We notice that MCTDH goes beyond Bose-Hubbard by picking out coupling between crossed states shown by sharp peaks in $\Delta\varepsilon$ at the corresponding values of $U^0$. Also, it is found that by raising the barrier height the first eigen-value crossing calculated with Bose-Hubbard converges to the MCTDH result.

We find in chapter 5 that knowledge of the low-lying eigenstates is crucial to understanding tunnelling dynamics in the double well. By initially preparing all particles to a single well we observe the effect known as quantum sloshing. We have demonstrated that oscillations corresponding to collective tunnelling between wells are found in the uncorrelated regime and again in the NOON regime with a much longer period, whereas tunnelling dynamics between these regimes are governed by several frequencies. This behaviour is explained by considering the contributions of the low-lying eigen-states.

As for thoughts of future work, first and foremost we would like to push for higher particle numbers. Computational time for $N$ particles scales as $N^3$ so we are restricted to systems where $N \approx 5$. In this thesis we have used at most three particles and while this is useful for understanding the physics it is hard to achieve experimentally. In this regard a generalisation of the rescaling scheme found in chapter 3 may assist MCTDH in reaching particle numbers greater than five. In further work it would be interesting to study what effect tilting the double well has on tunnelling dynamics. Our discussion only considered tilting the potential to prepare the system. However, asymmetry exists in experiment and may be used to find tunnelling resonances, where tunnelling is much faster and NOON states are protected from fluctuations of the systems potential [23].

Appendix A

# Two-Mode Analysis of Dynamics in the Double-Well

In chapter 2.7 we considered quantum sloshing in the double well. Here we present further calculations omitted from the text.

## A.1 Probability

In this section we summarise a result found in the appendix of [24] to calculate the probability of finding all particles in the right well at some time $t$. The initial state can be expanded into the energy eigen-basis

$$|\Psi(0)\rangle \;=\; |0,N\rangle \;=\; \sum_{k=0}^{N} c_0^k |\phi_0^k\rangle\,, \tag{A.1}$$

where $|\phi^k\rangle = \sum_{n_L=0}^{N} c_{n_L}^k |n_L, N-n_L\rangle$ are the eigen-states of $\hat{H} = -J\sum_{j\neq j'} \hat{b}_j^\dagger \hat{b}_{j'}$ with associated eigen-values $\varepsilon^k = -J(N-2k)$. The coefficients $c_{n_L}^k$ are obtained via [24]

$$c_{n_L}^k = \langle n_L, N-n_L|\phi_{n_L}^k\rangle = A^k H^k \langle n_L|N\rangle \sqrt{P_{1/2}\langle n_L|N\rangle}\,, \tag{A.2}$$

where

$$\begin{aligned} P_{1/2}\langle n_L|N\rangle &= \frac{1}{2^N}\frac{N!}{n_L!(N-n_L)!}\,, \\ A^k &= \sqrt{\frac{(N-k)!}{k!N!}}\,, \end{aligned} \tag{A.3}$$

and $H^k\langle n_L|N\rangle$ are the discrete Hermite polynomials satisfying

$$\begin{aligned} H^0\langle n_L|N\rangle &= 1 \\ H^1\langle n_L|N\rangle &= 2(N/2-n_L)H^0\langle n_L|N\rangle \\ H^{k+1}\langle n_L|N\rangle &= 2(N/2-n_L)H^k\langle n_L|N\rangle - k(N-k+1)H^{k-1}\langle n_L|N\rangle\,. \end{aligned} \tag{A.4}$$

Therefore we can write

$$H^k\langle 0|N\rangle = \frac{N!}{(N-k)!}\,. \tag{A.5}$$

Eq. (A.1) becomes

$$|0,N\rangle = \sum_{k=0}^{N}\sqrt{P_{1/2}\langle k|N\rangle}|\phi_0^k\rangle\,. \tag{A.6}$$

The probability of finding all particles in the right well is

$$\begin{aligned} P_{n_L}(t) &= \Big|\langle 0,N|e^{-iHt}|\Psi(0)\rangle\Big|^2 \\ &= \Big|\frac{1}{2^N}\sum_{k=0}^{N}\frac{N!}{k!(N-k)!}e^{iJ(N-2k)t}\Big|^2 \\ &= \Big|\frac{1}{2^N}\sum_{k=0}^{N}\frac{N!}{k!(N-k)!}(e^{-iJt})^k(e^{iJt})^{(N-k)}\Big|^2\,. \end{aligned} \tag{A.7}$$

Making use of the binomial theorem and Euler's formula we find

$$\begin{aligned} P_{n_L}(t) &= \Big|\frac{1}{2^N}(e^{-iJt}+e^{iJt})^N\Big|^2 \\ &= \cos^{2N}(Jt)\,. \end{aligned} \tag{A.8}$$

## A.2 Time Dependent Number Operator (Heisenberg Picture)

We can find the number of atoms in the left well at any time $t$ with

$$n_L = \underbrace{\langle\Psi(t)|a_L^\dagger}_{A}\underbrace{a_L|\Psi(t)\rangle}_{B}\,. \tag{A.9}$$

To simplify this equation we first expand $B$.

$$\begin{aligned} B &= \frac{1}{2^{N/2}\sqrt{N!}}\, a_L \left[a_L^\dagger \cos(Jt) + a_R^\dagger \sin(Jt)\right]^N |vac\rangle \\ &= \frac{1}{2^{N/2}\sqrt{N!}} \left[\cos(Jt) + \left(a_L^\dagger \cos(Jt) + a_R^\dagger \sin(Jt)\right) a_L \left(a_L^\dagger \cos(Jt) + a_R^\dagger \sin(Jt)\right)^{N-1}\right] |vac\rangle \\ &= \frac{1}{2^{N/2}\sqrt{N!}} \sum_{q=0}^{N-1} \left(a_L^\dagger \cos(Jt) + a_R^\dagger \sin(Jt)\right)^q \cos(Jt)\, |vac\rangle\,. \end{aligned} \tag{A.10}$$

A similar expression is found for A and Eq. (A.9) becomes

$$\begin{aligned} n &= \frac{1}{2^N N!} \sum_{p,q=0}^{N-1} \langle vac| \left(a_L \cos(Jt) + a_R \sin(Jt)\right)^p \left(a_L^\dagger \cos(Jt) + a_R^\dagger \sin(Jt)\right)^q |vac\rangle \cos^2(Jt) \\ &= N \cos^2(Jt)\,. \end{aligned} \tag{A.11}$$

# Bibliography


[1] K.B. Davis, M.O. Mewes, M.R. Andrews, N.J. van Druten, D.S. Durfee, D.M. Kurn, and W. Ketterle, *Bose-einstein condensation in a gas of sodium atoms*, Physical Review Letters **75**, 3969–3973 (1995).

[2] M.H. Anderson, J.R. Ensher, M.R. Matthews, C.E. Wieman, and E. Cornell, *Observation of Bose-Einstein condensation in a dilute atomic vapor*, Science(Washington) **269**, 198–198 (1995).

[3] B.L. Tolra, K.M. OHara, J.H. Huckans, W.D. Phillips, S.L. Rolston, and J.V. Porto, *Observation of reduced three-body recombination in a correlated 1D degenerate Bose gas*, Physical Review Letters **92**, 190401 (2004).

[4] M. Albiez, R. Gati, J. Fölling, S. Hunsmann, M. Cristiani, and M.K. Oberthaler, *Direct observation of tunneling and nonlinear self-trapping in a single bosonic Josephson junction*, Physical Review Letters **95**, 10402 (2005).

[5] J. Dunningham, K. Burnett, and W.D. Phillips, *Bose–Einstein condensates and precision measurements*, Philosophical Transactions A **363**, 2165 (2005).

[6] N.S. Ginsberg, S.R. Garner, and L.V. Hau, *Coherent control of optical information with matter wave dynamics*, Nature **445**, 623–626 (2007).

[7] A. Görlitz, J.M. Vogels, A.E. Leanhardt, C. Raman, T.L. Gustavson, J.R. Abo-Shaeer, A.P. Chikkatur, S. Gupta, S. Inouye, T. Rosenband, et al., *Realization of Bose-Einstein condensates in lower dimensions*, Physical Review Letters **87**, 130402 (2001).

[8] L. Tonks, *The complete equation of state of one, two and three-dimensional gases of hard elastic spheres*, Physical Review **50**, 955–963 (1936).

[9] M. Girardeau, *Relationship between systems of impenetrable bosons and fermions in one dimension*, Journal of Mathematical Physics **1**, 516 (1960).

[10] L.D. Landau and E.M. Lifshitz, **Statistical Physics: Course of Theoretical Physics, Vol. 5** (Pergamon, 1980).

[11] W. Ketterle and N.J. Van Druten, *Bose-Einstein condensation of a finite number of particles trapped in one or three dimensions*, Physical Review A **54**, 656–660 (1996).

[12] F. Schwabl, **Advanced quantum mechanics** (Springer Verlag, 2008).

[13] M. Olshanii, *Atomic scattering in the presence of an external confinement and a gas of impenetrable bosons*, Physical Review Letters **81**, 938–941 (1998).

[14] T. Busch, B.G. Englert, K. Rzażewski, and M. Wilkens, *Two cold atoms in a harmonic trap*, Foundations of Physics **28**, 549–559 (1998).

[15] J. Goold and T. Busch, *Ground-state properties of a Tonks-Girardeau gas in a split trap*, Physical Review A **77**, 63601 (2008).

[16] M. Abramowitz and I.A. Stegun, **Handbook of mathematical functions with formulas, graphs, and mathematical tables** (Dover Publications, 1964).

[17] H.D. Meyer, F. Gatti, and G.A. Worth, **Multidimensional quantum dynamics: MCTDH theory and applications** (Wiley-VCH, 2009).

[18] C. Pethick and H. Smith, **Bose-Einstein condensation in dilute gases** (Cambridge University Press, 2002).

[19] L.P. Pitaevskiĭ and S. Stringari, **Bose-Einstein condensation** (Oxford University Press, 2003).

[20] M.H. Beck, A. Jackle, G.A. Worth, and H. Meyer, *The multiconfiguration time-dependent Hartree (MCTDH) method: A highly efficient algorithm for propagating wavepackets*, Physics Reports **324**, 1 (2000).

[21] H.D. Meyer and G.A. Worth, *Quantum molecular dynamics: propagating wavepackets and density operators using the multiconfiguration time-dependent Hartree method*, Theoretica Chimica Acta **109**, 251–267 (2003).

[22] D.R. Dounas-Frazer, A.M. Hermundstad, and L.D. Carr, *Ultracold Bosons in a Tilted Multilevel Double-Well Potential*, Physical Review Letters **99**, 200402 (2007).

[23] L.D. Carr, D.R. Dounas-Frazer, and M.A. Garcia-March, *Dynamical realization of macroscopic superposition states of cold bosons in a tilted double well*, Europhysics Letters **90**, 10005 (2010).

[24] D. Dounas-Frazer. *Ultracold bosons in a multi-dimensional, tilted, double-well trap.* Master's thesis, Colorado School of Mines, 2007.

[25] S. Zöllner, **One-dimensional Few-boson Systems in Single-and Double-well Traps**, D.Phil thesis, University of Heildelberg, 2008.

[26] E. Caurier, G. Martinez-Pinedo, F. Nowacki, A. Poves, and A.P. Zuker, *The shell model as a unified view of nuclear structure*, Reviews of Modern Physics **77**, 427–488 (2005).

[27] K. Suzuki and S.Y. Lee, *Convergent theory for effective interaction in nuclei*, Progress of Theoretical Physics **64**, 2091–2106 (1980).

[28] J. Christensson, C. Forssén, S. Åberg, and S.M. Reimann, *Effective-interaction approach to the many-boson problem*, Physical Review A **79**, 12707 (2009).

[29] D.W. Hallwood, T. Ernst, and J. Brand. *Robust mesoscopic superposition of strongly correlated ultracold atoms.* Aug 2010.